



# HHS Public Access

Author manuscript

*Nano Today*. Author manuscript; available in PMC 2019 August 01.

Published in final edited form as:

*Nano Today*. 2018 August ; 21: 106–125. doi:10.1016/j.nantod.2018.06.006.

## Ultrasmall Noble Metal Nanoparticles: Breakthroughs and Biomedical Implications

Xingya Jiang, Bujie Du, Yingyu Huang, and Jie Zheng\*

Department of Chemistry and Biochemistry, The University of Texas at Dallas, 800 West Campbell Road, Richardson, Texas 75080, USA.

### Abstract

As a bridge between individual atoms and large plasmonic nanoparticles, ultrasmall (core size <3 nm) noble metal nanoparticles (UNMNPs) have been serving as model for us to fundamentally understand many unique properties of noble metals that can only be observed at an extremely small size scale. With decades' efforts, many significant breakthroughs in the synthesis, characterization and functionalization of UNMNPs have laid down a solid foundation for their future applications in the healthcare. In this review, we aim to tightly correlate these breakthroughs with their biomedical applications and illustrate how to utilize these breakthroughs to address long-standing challenges in the clinical translation of nanomedicines. In the end, we offer our perspective on the remaining challenges and opportunities at the frontier of biomedical-related UNMNPs research.

### Keywords

Ultrasmall nanoparticles; Noble metal nanoparticles; Physical properties; Physiological properties; Biomedical applications

### Introduction

Among all the engineered nanoparticles developed today, ultrasmall noble metal nanoparticles (UNMNPs), defined as noble metal nanoparticles with core size less than 3nm, have been drawing extensive attentions from researchers for more than half a century because not only did they serve as unique platforms to study the size-dependencies at an extremely small size scale that are often hard to achieve with other nanomaterials but they also opened new pathways to address many challenges in areas such as energy and healthcare. Compared to semiconductor quantum dots, UNMNPs also have a long history of serving as model for the fundamental understandings of quantum-size effects in nanomaterials. These understandings were significantly advanced by many breakthroughs in the synthesis and characterization of UNMNPs, which eventually lead to various practical

\* jiezheng@utdallas.edu.

**Publisher's Disclaimer:** This is a PDF file of an unedited manuscript that has been accepted for publication. As a service to our customers we are providing this early version of the manuscript. The manuscript will undergo copyediting, typesetting, and review of the resulting proof before it is published in its final citable form. Please note that during the production process errors may be discovered which could affect the content, and all legal disclaimers that apply to the journal pertain.



## Breakthrough in the synthesis of UNMNPs

### Precisely size-controlled synthesis

Heterogeneity in size is generally considered an intrinsic property of nanomaterials, which, however, has been a serious road block in the clinical translation of nanomedicines because heterogenous size distribution can create many uncertainties in reproducing nanomedicines with the same therapeutic efficacy on the large scale. Thus, precise control of nanomaterials with size down to atomic level is highly appreciated, which has also been a long journey for chemists. To date, gold[13–23], silver[24–26], platinum[27, 28], palladium[29, 30], and iridium[31] nanoparticles have been all successfully synthesized with atomic monodispersity. These synthesized nanoparticles often comprise several to dozens of atoms and therefore termed as “nanocluster”. Among all these noble metal nanoclusters, gold nanoclusters (AuNCs) are the most extensively studied and many established theories and synthesis methodologies are also derived from the investigation of AuNCs, so we mainly focus on AuNCs in summarizing the breakthrough of precisely size-controlled synthesis. For other types of noble metal nanoclusters, like AgNCs, readers can refer to the indicated reviews[32–35].

The efforts on the precise control of the sizes of gold nanoparticles can be dated back to 1970s-80s when a series of AuNCs ( $\text{Au}_5$ ,  $\text{Au}_8$ ,  $\text{Au}_{10}$ ,  $\text{Au}_{11}$ ,  $\text{Au}_{13}$  and  $\text{Au}_{55}$ ) protected by weakly bound ligands (e.g. phosphine) were synthesized and characterized[36–40]. Among these AuNCs,  $\text{Au}_{13}$  and  $\text{Au}_{55}$  clusters were found to be particularly stable, enabling researchers to further investigate their other exciting properties. The special stability of  $\text{Au}_{13}$  and  $\text{Au}_{55}$  can be explained by the theory of “full-shell clusters”, which are particles comprised of a central atom and then fully covered by shells of atoms that end up in perfect outer geometries (generally in close-packed icosahedral arrangements, the number of atoms per shell equals to  $10n^2+2$ , where  $n$  is shell number; so that the total number of atoms for one-shell cluster is  $1+12=13$  and  $13+42=55$  for two-shell cluster *etc.*)[29, 41]. Not limited to gold clusters, full-shell clusters of other metals, such as rhodium, platinum and palladium, were also discovered[42–44]. While early studies of Au clusters with well-defined sizes greatly advanced our fundamental understandings of UNMNPs at an extremely small size scale, the detailed atomic arrangement of these clusters could not be unraveled with single crystal X-ray analysis due to the low stability[41]. In 2007, the successful synthesis and total structure determination of  $\text{Au}_{102}(\text{pMBA})_{44}$  (pMBA = paramercaptobenzoic acid) make it possible to unravel how exactly gold atoms are packed together[45]. This breakthrough indicates it is feasible to synthesize much larger Au clusters with precise size control. In the past decade, major effort for the preparation of atomically precise AuNCs has been dedicated to achieving the goal of “one batch, one size” without laborious post-synthetic separation. Jin et al. established the “size-focusing” methodology in synthesizing atomically precise AuNCs, which involves two key steps, first the Au(I)-SR complexes are reduced to a relatively narrow size distribution around the target size via kinetically controlled reduction methods, and then the resulting mix-sized AuNCs are subject to an aging process that converts the thermodynamically unfavored different-sized AuNCs to the thermodynamically favored target size nanocluster, the so-called “size-focusing” step. Using this method, atomically monodisperse  $\text{Au}_{25}(\text{SR})_{18}$ [13, 14],  $\text{Au}_{38}(\text{SR})_{24}$ [15, 16],  $\text{Au}_{64}(\text{SR})_{32}$ [17],

Au<sub>99</sub>(SR)<sub>42</sub>[18], Au<sub>144</sub>(SR)<sub>60</sub>[19] and Au<sub>333</sub>(SR)<sub>79</sub>[20] have been directly synthesized with high yield.

Although these Au clusters with precise size control have greatly advanced our fundamental understandings of gold-gold and gold ligand interactions, they are only dissolved in organic solvents, precluding them from many biomedical applications. To address this challenge, significant efforts have been dedicated to synthesizing aqueous soluble Au clusters with well-defined number of gold atoms. In 1998–2000, Whetten et al. synthesized a class of glutathione (GSH) coated Au clusters with core sizes ranging from 4kDa to 14kDa and observed the core-size-dependent optical properties from these water-soluble Au clusters[46, 47]. After gel electrophoresis separation, Au<sub>28</sub>(SG)<sub>16</sub> clusters were successfully obtained. However, it should be noted that Au<sub>28</sub>(SG)<sub>16</sub> later was corrected to be Au<sub>25</sub>(SG)<sub>18</sub>. In 2003, Zheng et al. utilized PAMAM dendrimers, a unique category of branched polymers with well-defined molecular weights, to encapsulate ultrasmall gold nanoclusters with strong blue emission through a one-step synthesis at high purity[48]. With the assistance of electrospray ionization mass spectrometry (ESI-MS), this blue-emitting gold nanocluster was identified as monodispersed Au<sub>8</sub> clusters. Since 2003, many other different sized water-soluble Au clusters with precise number of atoms have been synthesized. For instance, Xie et al. developed a scalable synthesis method using gaseous carbon monoxide (CO) as a mild reducing agent to produce a set of atomically precise AuNCs (Au<sub>10–12</sub>, Au<sub>15</sub>, Au<sub>18</sub> and Au<sub>25</sub>) capped by two different water-soluble ligands, GSH and 3-mercaptopropionic acid (MPA)[21]. The different sized AuNCs were selectively formed simply by varying the pH of reaction solution to fine-tune the reaction kinetics. Similarly, borane *tert*-butylamine (TBAB) [22] and sodium cyanoborohydride (NaBH<sub>3</sub>CN)[23] have all been exploited as mild reducing agents for the high yield synthesis of GSH protected Au<sub>15</sub> and Au<sub>18</sub> nanoclusters. Template method serves as another viable way to form water-soluble nanoclusters with well-controlled size, biomolecules such as protein[49–51], DNA[52, 53] and biocompatible dendrimers, like poly(amidoamine) (PAMAM)[48, 54] have been reported as valuable templates to form Au and Ag nanoclusters with defined number of metal atoms. In addition to the direct synthesis from gold salt precursors, atomically precise AuNCs can also be obtained through a “top-down” approach, where original AuNPs/AuNCs are transformed to new types of AuNCs via chemical etching with excess thiol ligands under thermal conditions[55–57].

After examining the current synthetic methods to the atomically precise thiolated AuNCs, three commonalities can be found. Firstly, the feeding ratio of thiol ligands to Au(III) precursors is large (usually 3–6), which ensures the complete conversion of Au(III) to Au(I)-ligand complex (polymers) and enables fast protection/passivation of the newly formed AuNCs in the subsequent reduction process to avoid aggregation. Secondly, a controlled (slow) reduction kinetics through either the use of mild reducing agent or changing the physical parameters (low temperature, drop-wise addition, phase transfer, *etc.*). Thirdly, the creation of a unique environment that favors the formation of a certain sized AuNCs, such as different pH, temperature or solvent. These empirical rules may offer guidance for the synthesis of other noble metal nanoclusters with well controlled sizes. To gain more fundamental understanding of the precise synthesis and facilitate the development of new synthetic strategies, both experimental and theoretical studies have been devoted to

unraveling the growth mechanism of AuNCs[58–62], which has shed some light on the Au(I)-ligand complex formation as well as the subsequent nucleation, growth and size-focusing processes. Though atomically monodispersed UNMNPs are beneficial to the reproducibility and future good manufacturing practice (GMP) production of nanomedicines, it should be pointed out that currently most UNMNPs used in biomedical research, as will be mentioned in later sections, are not yet atomically precise. More in-depth research and development is still in great demand to establish more facile and versatile approaches for the preparation of different kinds of UNMNPs with atomically precise monodispersity.

### Biomedical applications enabled by precise size-control of UNMNPs

The breakthrough in atomic level size-controlled synthesis of UNMNPs offers researchers many opportunities to study the bionano interactions with unprecedented precision. As size is one of the key factors influencing nanoparticle behaviors *in vivo*, atomically precise UNMNPs first serve as ideal tools to probe the size-related interactions between nanoparticles and biological system with such atomic resolution that are currently impossible using other nanomaterials. For example, Zheng et al. recently discovered an unusual kidney filtration trend in the sub-nanometer size regime using a series of GSH protected AuNCs (Au<sub>25</sub>, Au<sub>18</sub>, Au<sub>15</sub> and Au<sub>10–11</sub>)[63]. Unlike traditional view of kidney glomerular filtration barrier, a “size cutoff” slit that rapidly excretes nanoparticles smaller than kidney filtration threshold (KFT, ~6nm), they found that, surprisingly, kidney glomeruli behave as an atomically precise barrier to slow down the renal clearance of smaller nanoparticles when their sizes are reduced to sub-nanometer range (Fig. 2A). Compared to that of Au<sub>25</sub>(~1nm), just few-atom decreases in size (Au<sub>18</sub>, Au<sub>15</sub> and Au<sub>10–11</sub>) can result in 4–9 times reductions of the initial renal clearance efficiency. This trend was found not just for glomerular filtration but also applies to normal blood vessel extravasation and could be used to enhance the passive tumor targeting of sub-nanometer AuNCs through the enhanced permeability and retention (EPR) effect. These discoveries highlight how precisely the body could respond to the size variance of ultrasmall AuNPs and also imply precise size-control should be the prerequisite for other *in vivo* comparisons made in this ultrasmall size range. Ackerson et al. studied the effect of ligand replacement on the biodistribution, pharmacokinetics and elimination of Au<sub>25</sub>(SG)<sub>18</sub> and Au<sub>102</sub>(pMBA)<sub>44</sub> nanoclusters[64]. They found that apart from the widely recognized parameters such as net surface charge and hydrodynamic diameter, the surface charge density, exposed hydrophobic surface and surface structure also profoundly impact the *in vivo* behavior of nanoparticles (Fig. 2B). The ligand effect of atomically precise AuNCs on cellular uptake and cell metabolism was also investigated[65].

The ability of precisely controlling the size of UNMNPs also enables the exploitation of their size-related properties. Au<sub>25</sub>(SR)<sub>18</sub> nanoclusters were shown to efficiently generate singlet oxygen upon photo excitation and have the potential for photodynamic therapy (Fig. 2C)[66]. Au<sub>10–12</sub>(SG)<sub>10–12</sub> nanoclusters have been demonstrated as an excellent radiosensitizer for cancer radiotherapy[67]. The 1.4nm phosphine-stabilized Au<sub>55</sub> nanoclusters were found to be particularly cytotoxic compared to that of other-sized Au nanoparticles ranging from 0.8–15nm due to size-dependent coordination with DNA,

making Au<sub>55</sub> a potential anticancer drug[68]. Recently, 6-mercaptohexanoic acid (MHA) capped Au<sub>25</sub> nanoclusters were reported to have antimicrobial functions, which are distinct from the bio-inertness that larger MHA-AuNPs (>2nm) exhibit[69]. The surprising wide-spectrum antimicrobial activity is a size-dependent phenomenon and only occurs to ultrasmall AuNCs. Moreover, UNMNPs of certain sizes often possess photoluminescent characters, such as Au<sub>5</sub>[54], Au<sub>8</sub>[48], Au<sub>22</sub>[70], Au<sub>23</sub>[56], Au<sub>25</sub>[71], Ag<sub>9</sub>[72], Ag<sub>14</sub>[73], Pt<sub>5</sub>[27] and Pt<sub>8</sub>[74] nanoclusters, which can be developed as *in vitro*[27, 73, 74] and *in vivo*[70, 75] imaging agents, as well as various optical sensors[71, 72, 76]. More applications of luminescent noble metal nanoclusters in bioimaging and biosensing can be found in other review articles[35, 77–79]. In addition, some magic sized Ag[80, 81] and Au[82–84] nanoclusters exhibit much stronger two-photon absorption and fluorescence compared with conventional two-photon organic dyes, making them excellent candidates for biolabeling and bioimaging. Electrogenerated chemiluminescence (ECL) with efficient and sustainable near infrared (NIR) emission was reported for Au<sub>22</sub>[85], Au<sub>25</sub>[86, 87], Au<sub>38</sub>[88] and Au<sub>144</sub>[89] nanoclusters (Fig. 2D), which are superior to semiconductor quantum dot based ECL in terms of the emission efficiency and biosafety and show great potential in areas such as bioimaging and biosensing[90, 91]. Similar ECL phenomenon was also observed in Ag nanoclusters but with shorter emission wavelength[92, 93].

### Doping or alloying UNMNPs

In the field of material science, extending or improving the properties of some materials (metal, semiconductor, *etc.*) through doping foreign elements bears a long history. Due to the synergistic effect, the resulting alloys often exhibit enhancements in specific properties or show new properties that are missing in the original materials[94]. However, doping and alloying UNMNPs for the application in biomedical research starts to boom only in the recent decade and is gaining increasing interest. Here, we briefly summarize the current strategies to synthesize colloidal doped or alloyed UNMNPs and their biomedical related applications. With respect to the terminology, “doping” usually refers to a specific number of heteroatoms being introduced to the noble metal nanoparticle (especially atomic precise nanocluster), whereas “alloying” refers to a range of heteroatoms[95]. One of the commonest chemical methods for the preparation of alloying (doping) UNMNPs is co-reduction of noble metal salt along with the heterometal salt in the presence of protecting ligands. The elemental ratios of the final products can be tuned by changing the feeding salt ratios and their sizes are controlled through reaction parameters (reducing agent, protecting ligand, temperature, solvent, *etc.*). Using this method, ultrasmall alloying nanoparticles such as Ag-Au[96–98], Pd-Au[99], Cu-Au[100, 101]; Ag[102, 103], Cu[102, 104], Pt[105, 106], Pd[107, 108] doped AuNCs and Ni[109], Pd[110], Pt[110, 111] doped AgNCs have been successfully fabricated. The preferential formation of certain final products depends largely on their structural or electronic stabilities. Another way to dope or alloy UNMNPs is through “post-synthesis treatment”, which incorporates foreign atoms into pre-synthesized monometallic nanoparticles. Galvanic replacement, for example, is an effective way to dope metal atoms onto pre-existing nanoparticles. The galvanic replacement utilizes redox potential difference between the metals in nanoparticles and the doping metal ions, which possess a higher redox potential and thus can be reduced and deposited on the surface of nanoparticles. As the AuCl<sub>4</sub><sup>-</sup>/Au (~1V) is higher than Pd<sup>2+</sup>/Pd (~0.95V) and Ag<sup>+</sup>/Ag

( $\sim 0.8\text{V}$ ) in redox potential[112], Au-Pd[113] and Au-Ag[114–116] alloying nanoparticles can be prepared by mixing chloroauric acid ( $\text{HAuCl}_4$ ) with the corresponding nanoparticles. Of note, anti-galvanic replacement, though appears thermodynamically unfavorable, is observed recently in UNMNPs. Ag and Cu doped AuNCs produced by simply reacting  $\text{Ag}^+$  and  $\text{Cu}^{2+}$  with ultrasmall AuNCs have been reported by Wu et al. and the unusual reducing ability of AuNCs is thought to be size-related[117]. Later on, the similar anti-galvanic doping of  $\text{Cu}^{2+}$  onto AgNCs[118] and  $\text{Hg}^{2+}$  onto AuNCs[119] were also found. However, the detailed mechanism underlying anti-galvanic replacement remains to be clarified. In addition to the commonly used preparation routes mentioned above, molecular beam, thermal decomposition, electrochemical synthesis and radiolysis are all able to produce alloyed UNMNPs and readers are directed to dedicated reviews for further information[94, 120].

### Biomedical applications enabled by doping or alloying UNMNPs

Doping and alloying UNMNPs have led to many exciting biomedical applications, among which nuclear medicine imaging is particularly attractive. Nuclear medicine imaging techniques such as single photon emission computed tomography (SPECT) and positron emission tomography (PET) have the advantages of functional imaging, high sensitivity, accuracy and unlimited tissue penetration that make them one of the most popular diagnostic tools in clinical practice. One of the early examples is to dope  $^{198}\text{Au}$  into ultrasmall luminescent AuNPs so that the limited light penetration depth in the clinical applications of luminescent AuNPs can be overcome by SPECT imaging (Fig. 3A), which opened a new pathway to integrate UNMNPs with clinically used imaging techniques and expedited their translation into the clinics[121].  $^{64}\text{Cu}$  is a favorable radiotracer that has suitable half-life (12.7h) and well-established coordination chemistry for subsequent linking to disease-targeting moieties, however, conventionally  $^{64}\text{Cu}$  is stabilized through chelating with macrocyclic chelators such as DOTA (1,4,7,10-tetraazacyclododecane-1,4,7,10-tetraacetic acid), which is metastable *in vivo* and can result in misinterpretation of images and unwanted radiation burden due to the transchelation of  $^{64}\text{Cu}$  to proteins[122]. Thus, directly incorporate  $^{64}\text{Cu}$  to nanoparticles, especially UNMNPs for efficient *in vivo* elimination, through doping or alloying is desired. Liu et al. successfully synthesized ultrasmall PEGylated  $^{64}\text{Cu}$ -Au alloy nanoparticles for cancer PET imaging[101]. This new PET imaging probe exhibited high stability, optimal biodistribution, efficient systemic clearance and could passively target prostate cancer in a mouse model. They later improved the probe by conjugating active targeting ligands (AMD3100) onto the  $^{64}\text{Cu}$ -Au alloy nanoparticles and demonstrated its ability to sensitively detect both the primary breast cancer and the lung metastasis through PET imaging (Fig. 3B and C)[123]. Chen et al. reported self-illuminating  $^{64}\text{Cu}$  doped AuNCs for PET and NIR dual-modality cancer imaging[124]. The doped radioactive  $^{64}\text{Cu}$  acts as both the energy donor to excite AuNCs via Cerenkov resonance energy transfer (CRET) and the positron-emitting source (Fig. 3D). Cerenkov luminescence (CL) based theranostic agent was also developed by doping radioactive  $^{198}\text{Au}$  to albumin coated AuNCs. The resulting radio-optical AuNCs exhibited NIR emission excited by CL and also served as radionuclide for cancer therapy[125]. In many cases, the luminescent properties of UNMNPs could be significantly enhanced after doping foreign atoms[126–130], enabling their applications in optical sensing[129, 131–134], *in vitro*[126, 135] and *in*

*vivo*[136] fluorescence imaging. In addition to practical applications, alloying UNMNPs also help to study some fundamental biomedical questions. Zheng et al. investigated the density effect of ultrasmall nanoparticles on their renal clearance and tumor targeting using a class of Au, Au/Ag alloy with two ratios and Ag ultrasmall nanoparticles of the same size and surface chemistry but different core densities[96]. They observed that increasing particle density would lead to higher tumor targeting efficiency and lower renal clearance in the early elimination phase due to density-dependent margination effect in the laminar flow of circulating nanoparticles.

## Breakthrough in understanding the physical properties of UNMNPs

### Structures of UNMNPs

The structure understanding of UNMNPs has progressed considerably in recent decade owing to the breakthroughs in their precisely chemical synthesis and the advancement of characterization methods. Atomically precise UNMNPs with molecular purity have enabled their crystallization and subsequent determination of their total structure through X-ray crystallography. To date, crystal structures of dozens of atomically precise UNMNPs (including alloying nanoparticles) have been reported since the first total structure determination of Au<sub>102</sub>(SR)<sub>44</sub> in 2007[45], and new structures are constantly emerging. Based on the current resolved structures, thiol protected UNMNPs generally can be seen as consisting of a metal kernel and surface capping motifs that bind to the metal kernel through metal-metal bond or metal-sulfur bond. The packing structure of kernel metal atoms can be various such as FCC (face-centered cubic), BCC (body-centered cubic), HCP (hexagonal close-packed) and icosahedron, depending on the metal type (Au vs. Ag) and cluster size. The surface capping motifs of Au nanoclusters are mainly staple-like Au<sub>n</sub>(SR)<sub>n+1</sub> oligomers or simple bridging thiolate –SR, however, for Ag nanoclusters more complex surface capping motifs are presented as each Ag atom can bind up to three –SR groups and each –SR to three Ag atoms, which makes the surface Ag-SR motifs adopt more complex 3-dimensional structures besides the simple oligomeric staples like those observed in AuNCs. These solved UNMNPs crystal structure information can provide valuable implications for their larger counterparts whose crystal structures are currently unavailable. Detailed review of the crystal structures for noble metal nanoclusters can be found elsewhere[137].

Though X-ray crystallography is the most accurate and straightforward way for total structure determination, single crystal growth of UNMNPs is not easy and most of the structure determined UNMNPs are organic soluble (hydrophobic). For many water-soluble UNMNPs that are hard to crystalize, nuclear magnetic resonance (NMR)[138–140], laser desorption ionization mass spectroscopy (LDI-MS)[138, 141], and X-ray absorption spectroscopy (XAS)[106, 142–145] are helpful tools to probe their structures. The local chemical environment of ligands revealed by <sup>1</sup>H NMR or <sup>13</sup>C NMR can be used to deduce the binding modes of surface ligands both qualitatively and quantitatively. Unlike the soft ionization methods in ESI-MS and matrix-assisted laser desorption/ionization (MALDI) mass spectrometry, which are frequently used to obtain the intact mass of clusters, the harsh ionization condition in LDIMS often leads to the breakdown of clusters to their stable subunits and important structure information can be drawn by analyzing their fragmentation



patterns. XAS is a powerful technique to probe the elemental, electronic and structural properties of UNMNPs in situ under variable conditions (solid or in solution, physical or chemical influences)[145]. A typical XAS spectrum is made up of two regions, X-ray absorption near edge structure (XANES) and extended X-ray absorption fine structure (EXAFS). XANES contains elemental and electronic information of the atoms in UNMNPs whereas EXAFS is rich in structural information and able to accurately reflect the local structure of the absorbing atom, such as the coordination number and bond distance[145, 146]. Jin et al. probed the structure of water-soluble Au<sub>25</sub>(SG)<sub>18</sub> nanoclusters using NMR in conjunction with LDI-MS and found that their structure is the same as that of Au<sub>25</sub>(SCH<sub>2</sub>CH<sub>2</sub>Ph)<sub>18</sub>[138]. They later revealed the relative stability of the two surface Au-S binding modes in Au<sub>25</sub>(SG)<sub>18</sub> by NMR and optical spectroscopy[139]. Zhang et al. did a series of investigations on the structural properties of UNMNPs using XAS, including the structure of thiol-protected or DNA-templated ultrasmall silver nanoclusters/nanoparticles[147–150], local structure of platinum nanoclusters[151, 152] and temperature-dependent bonding properties in gold nanoclusters[146, 153, 154]. More in-depth account of XAS and its applications in UNMNPs characterization can be found in recent reviews by Zhang et al.[145, 146].

### Biomedical applications from the unique structures of UNMNPs

Unraveling the structures of UNMNPs such as core geometries and ligand-binding modes can facilitate the understanding of their interactions with biomolecules. The strong binding between certain sized AuNCs with DNA [155] or proteins [156] were thought to be mediated by the unique core size/geometry enabled coordination with the local structures of those biomolecules (Fig. 4A and B). For example, phosphine protected Au<sub>55</sub> nanoclusters were experimentally verified a decade ago by Schmid et al. to interact with DNA strongly and exhibited cytotoxicity even higher than cisplatin in several cancer cell lines[157]. However, at that time Au<sub>55</sub>-DNA interaction was only studied by means of molecular-modeling simulations and elucidation of the exact coordination mode between Au<sub>55</sub> and the grooves of DNA was impossible due to the lack of Au<sub>55</sub> structures. With increasing Au<sub>55</sub> experimental structure information being uncovered in recent years[158, 159], it is anticipated that more detailed Au<sub>55</sub>-DNA interaction mechanism can be revealed, which would facilitate not only our comprehension of bio-nano interaction at molecular level but also the development of possible new drugs. Besides core structures, understanding the surface structures of UNMNPs is also critical as they directly interact with the surrounding environment. Zheng et al. discovered that the emission wavelength of ultrasmall luminescent AuNPs is closely related to the surface coverage and local binding structure of thiolate ligand (glutathione) on AuNPs[160]. High surface coverage and the resulting high degree of Au-S bonding as well as strong ligand-metal charge transfer would lead to shorter visible emission (~600nm), whereas low surface coverage, low degree of Au-S bonding and relatively weak ligand-metal charge transfer generate longer NIR emission (~810nm). By tuning the surface structures, these two colored emissions could be integrated into a single gold nanoparticle and the resulting dual-emissive AuNPs exhibit unique pH-dependent ratiometric emissions via energy transfer process (Fig. 4C). These findings offer new opportunities to modulate the photoluminescence of ultrasmall AuNPs for optimal bioimaging and quantitative pH sensing.

## Optical properties of UNMNPs

The fascinating optical properties of UNMNPs are some of the main reasons that make them so appealing to researchers. Compared to their larger counterparts, UNMNPs often exhibit several unique optical properties such as molecular-like absorption, strong photoluminescence (PL) and intrinsic chirality. Although some of these properties were observed decades ago, a giant leap has been made in regard to the understanding of their mechanisms in recent years. Because of the limited number of constituent metal atoms in UNMNPs, the typical localized surface plasmon resonance (LSPR) absorption of larger metal nanostructures is usually not presented due to the lack of sufficient free electrons needed for LSPR. Instead, two types of absorption are commonly observed for UNMNPs. One is step-like absorption (UV-Vis-NIR) profile with characteristic peaks resembling that of small molecules, reflecting the discrete (quantized) electronic energy levels in atomically monodisperse UNMNPs with few to more than one hundred of metal atoms (e.g., Au<sub>144</sub>(SR)<sub>60</sub>). The breakthrough in unraveling the crystal structures of these UNMNPs enables more accurately theoretical calculations that greatly advanced our understanding of their absorption spectra. For example, time-dependent density functional theory (TD-DFT) calculation of Au<sub>25</sub>(SR)<sub>18</sub> based on the resolved crystal structure correlates well with its experimental absorption spectrum and the origin of each characteristic peak can be understood by molecular orbital theories[161]. For thiolated Au and Ag nanoclusters, usually a selection rule-allowed HOMO-LUMO transition accounts for the lowest energy characteristic peak and these molecular orbitals involve significant contributions from both ligand (particularly the metal-binding sulfur atom) and metal atomic orbitals[161–163], indicating the important role of ligands in their electronic structures. The other commonly observed absorption is a featureless decay profile from UV to the NIR range, which usually indicates a mixture of different sized UNMNPs that can smear out the characteristic absorption peaks of their individual components due to size polydispersity. Of note, the absorption spectra of some monodispersed molecular-like UNMNPs may appear rather featureless under room temperature due to thermal broadening of the peaks, but fine and pronounced absorption structures can be revealed when measured at cryogenic conditions[164, 165]. The electronic properties of UNMNPs are also impacted by their surface chemistry. Even with the same ligand binding group such as thiolate, different tail groups (alkyl vs. aromatic)[166, 167] or alkane chain length[168] can modulate the electron density of metal cores through direct charge donation from the ligand to the metal and influence the electronic properties of UNMNPs, as determined by the UV/Vis absorption spectroscopy and conduction electron spin resonance spectroscopy.

Besides the interesting absorption character of UNMNPs, much effort has been devoted to understanding their fabulous PL. A large number of photoluminescent UNMNPs with impressive quantum yield were developed during the past 10–15 years and their emission spans from UV to the NIR spectrum range. Here we divide the PL of UNMNPs into two categories: one is fluorescence, characterized by a short lifetime (nanosecond scale) and small Stokes shift (usually <100nm); the other is phosphorescence with a large Stokes shift (>100nm) and long lifetime (microsecond scale) due to electron intersystem crossing and subsequent kinetically unfavored “triplet-to-singlet” transition. Strong fluorescence of UNMNPs mainly originate from the quantum confinement of metal free electrons (thus sp-

sp intraband transition), which is usually observed in few-atom metal nanoclusters without strong ligand-metal interactions, and the fluorescence excitation and emission wavelength are size-dependent. For instance, a series of PAMAM dendrimer encapsulated Au nanoclusters with different core atoms exhibit bright fluorescence ranging from UV ( $\text{Au}_5$ ) to NIR ( $\text{Au}_{31}$ ) and the dependence of emission energy on gold atom number can be well fitted with the free-electron (Jellium) model[54, 169]. The same mechanism also applies to many non-thiol protected few-atom fluorescent UNMNPs, including polymer-coated AuNCs[170], dendrimer-templated PtNCs[27] and DNA-templated AgNCs[171]. Thiol ligands are the commonest ligands used to protect UNMNPs as the strong metal-SR bond ensures a highly stable passivation of UNMNPs that is crucial for many bio-related applications. Phosphorescence is the dominant emission for thiolated UNMNPs, especially for NIR-emitting ones, and surface effect such as ligand-metal charge transfer usually plays a vital role in their luminescence mechanisms because of the strong interactions between thiolate ligands and metal atoms, rendering the excitation and emission of thiolated UNMNPs less size-dependent. Take glutathione coated ultrasmall AuNPs as examples,  $\text{Au}_{15}(\text{SG})_{13}$ ,  $\text{Au}_{18}(\text{SG})_{14}$ ,  $\text{Au}_{22}(\text{SG})_{16}$ ,  $\text{Au}_{25}(\text{SG})_{18}$ ,  $\text{Au}_{29}(\text{SG})_{20}$ ,  $\text{Au}_{39}(\text{SG})_{24}$  and ~2nm GS-AuNPs all show NIR emission in the 700–900nm range despite their distinct sizes[121, 172, 173]. Wang et al. systematically studied the NIR emissions from a series of monolayer-protected AuNCs of different thiolate ligands and core atoms, from which they found that the observed emissions were a result from the localized surface electronic states that depend on the type of core metal as well as the ligands attached to the metal surface rather than the size of metal core[174]. It should be noted that fluorescence and phosphorescence can coexist in a single nanoparticle due to the coexistence of multiple relaxation pathways within one nanoparticle, which is observed in some UNMNPs[175, 176]. The detailed PL origin and mechanism of UNMNPs are still not thoroughly clear and readers are advised to dedicated review and theoretical works for more discussion[177–179]. In addition to mechanism understanding, various strategies were developed to tune or improve the PL of UNMNPs. Methods such as increasing the rigidity of surface Au(I)-thiolate shell[180, 181], employing ligands with electron-rich atoms or groups[182] and conjugating proper chromophore to enable energy transfer[183] all have been proved to greatly enhance the quantum yield of Au nanoclusters. Modified bidentate thiol ligands (e.g., lipoic acid) were reported to endow luminescent Au nanoclusters with superb colloidal and photophysical stability and able to extend the emission wavelength beyond 1000nm for better *in vivo* imaging[83, 184].

Moreover, many UNMNPs show strong circular dichroism (CD) signals that manifest their chiral nature, which has sparked tremendous interest in exploring their chiroptical properties and potential applications. The chirality in these ultrasmall nanoparticles can originate from the ligands, either due to chiral ligands themselves[185, 186] or a chiral arrangement of achiral surface moieties[187, 188], or the intrinsically chiral metal core that is presented in some Au[189] and Ag[190] nanoclusters. Chiroptical properties not only exist at the ground state (as measured by CD spectroscopy) of UNMNPs but the excited state as well. Chiral AgNCs that possess both CD and circularly polarized luminescence (CPL) signatures were reported recently, where the chirality in ligand staples likely gave rise to the chiroptical activity in the emission states[191]. Chirality is also observed in alloying (doping) UNMNPs such as Au-Pd[192–194] and Au-Ag[195–197] nanoparticles. Understanding the

fundamentals of chirality in these ultrasmall nanosystems is indispensable for the advancement of future applications. For comprehensive account of nanoparticle chirality, some recent review articles are recommended[198, 199].

### Biomedical applications from the optical properties of UNMNPs

The remarkable optical properties of UNMNPs have given rise to a boom of their bio-related applications. The HOMO-LUMO electronic transition of some nanoclusters occurs at relatively lower energy (1.4eV~1.8eV) that results in a strong absorption peak in the NIR range, enabling them as NIR-light based photoacoustic and photothermal agents. For example, taking advantage of the NIR absorption of Au<sub>25</sub> nanocluster and its ability to generate singlet oxygen upon photoexcitation, Lin et al. developed a cancer theranostic platform by incorporating Au<sub>25</sub> nanoclusters into the mesoporous silica shell of upconversion nanoparticles and demonstrated the photoacoustic/thermal imaging-guided photothermal and photodynamic cancer therapy with single 808nm light irradiation (Fig. 5A)[200]. Au<sub>25</sub> functionalized magnetic metal-organic nanostructures were also reported to serve as a magnetic resonance imaging (MRI)-guided theranostic agent[201]. In addition to good photostability, the high population and long lifetime of triplet excited states in some UNMNPs allow an efficient energy transfer from the photoexcited UNMNPs to the surrounding ground state (triplet) oxygen molecules to form reactive singlet oxygen, making those UNMNPs excellent photosensitizers for photodynamic therapy, such as certain Ag[202] and Au[203, 204] nanoclusters reported recently. The luminescence of many thiolated UNMNPs is heavily associated with their surface settings, implying that minor perturbation (e.g., oxidation, reduction, protonation) of the surface conditions may lead to dramatic changes in their luminescence, which forms the foundation for various UNMNPs-based fluorescent sensors[205, 206]. Because of the involvement of ligand-metal charge transfer, the typical lifetime (0.1–10 μs) of thiolated luminescent UNMNPs is several orders of magnitude longer than that of biological autofluorescence (usually <10 ns)[207], making them attractive candidates for fluorescence lifetime bioimaging. Lifetime-based imaging holds several unique advantages compared with intensity-based imaging, including the independence of probe concentration and excitation intensity. Since fluorescence lifetime is sensitive to local environment (temperature, dynamic quenchers *etc.*), it can be also used as indicator (sensor) to probe the local variation of these factors. Nienhaus et al. reported cellular fluorescence lifetime imaging using long-lifetime NIR-emitting ultrasmall AuNPs[208]. Not only the internalization of AuNPs but also the different local environment between plasma membrane and intracellular space as well as the heterogeneity inside cells could be clearly revealed by fluorescence lifetime imaging without autofluorescence interference. They later further applied fluorescence lifetime imaging in intracellular temperature sensing and developed the ultrasmall AuNPs-based intracellular thermometry that enables high sensitivity temperature measurements within cells in a spatially resolved manner (Fig. 5B)[209]. UNMNPs with long emission lifetime also act as ideal probes for time-gated fluorescence bioimaging, which could significantly reduce the interference of short-lived tissue autofluorescence and greatly improve signal-to-noise ratio by only capturing the emission signal from a specific delayed time window after excitation[210, 211]. For *in vivo* fluorescence imaging, UNMNPs with higher quantum yield and longer emission wavelength (e.g. in the second NIR window 1000–1350nm) are desired. Highly

luminescent water-soluble Au<sub>22</sub> nanoclusters with a quantum yield (QY) of 42% were synthesized by Lee et al. and applied to *in vivo* imaging[212]. The unprecedented high QY for NIR-emitting thiolated AuNCs was achieved by simultaneously rigidifying the gold shell of Au<sub>22</sub> via surface conjugation with strong  $\pi$  -  $\pi$  stacking molecules (benzyl chloroformate) and enabling resonance energy transfer from the conjugated ligands (folate) to Au<sub>22</sub> nanoclusters (Fig. 5C). Zwitterionic bidentate thiol ligands protected ultrasmall AuNPs were recently reported to have extended emission up to 1300nm with appreciable QY[213]. *In vivo* imaging using these long emission-wavelength AuNPs exhibits improved contrast and resolution due to reduced photon scattering in tissues when comparing to that of conventional NIR (<900nm) imaging (Fig. 5D). Chirality serves as an important aspect of specific molecular recognition within biosystem and is crucial for areas such as pharmaceuticals and agrochemicals. UNMNPs-based biomolecule chiral recognition and enantiomer sensing were demonstrated recently, through either the individual nanoparticles[197] or their three-dimensional assembly[214].

## Breakthrough in understanding the physiological properties of UNMNPs

### In vivo stability and clearance pathway

For UNMNPs used *in vivo*, their stability in the body is of paramount importance as it directly affects the pharmacokinetics, biodistribution, clearance profile and toxicity of UNMNPs. Both the core metal and surface ligands influence the *in vivo* stability of UNMNPs. Compared to metals (e.g., Au, Pt) with the highest nobility, nanoparticles composed of less noble metals (e.g., Ag, Cu) tend to be less stable *in vivo* due to their reduced chemical inertness[215, 216]. AgNPs, for example, are well known to be subject to oxidative dissolution and gradually release Ag<sup>+</sup> ions in aqueous medium, particularly in *in-vivo* conditions where high levels of Ag<sup>+</sup>-binding ligands (Cl<sup>-</sup>, thiols, proteins, *etc.*) are presented[217, 218]. The dissolution rate of AgNPs can be modulated by many factors such as size, oxidant availability and surface coating[219]. AgNPs protected by thiol ligands show significantly suppressed Ag<sup>+</sup> releasing rate and are therefore frequently used for *in vivo* purpose. Besides the degradation of metal core, opsonization of UNMNPs through non-specific binding with endogenous biomolecules (e.g., serum proteins) is another key factor determining their *in vivo* stability and also one of the greatest challenges facing their clinical translation. Fast opsonization leads to UNMNPs being rapidly recognized by the immune system and subsequent uptake by the mononuclear phagocyte system (MPS, like liver, spleen, bone marrow, *etc.*). Meanwhile, binding to proteins, like serum albumin, would significantly increase the effective size of UNMNPs *in vivo* to such an extent that they can not be filtered through kidney despite their ultrasmall small size *in vitro*, which, along with the rapid MPS uptake, result in the accumulation of UNMNPs in healthy tissues and generate toxicity concerns. Nanoparticle-protein interaction is one of the most studied bio-nano interactions in the past decade as it often represents the biological identity of nanoparticles *in vivo* and profoundly affects their *in vivo* behaviors, such as cellular uptake[220], tumor targeting[221] and immunogenicity[222]. However, most of the investigations are based on larger (core size >3nm) nanoparticles and ultrasmall nanoparticles may interact with proteins differently in some aspects. Unlike the usually referred “protein corona” for larger nanoparticles where multiple proteins can adsorb onto

the surface of a single nanoparticle, UNMNPs, because of their extremely small sizes that are comparable or even smaller than that of the typical proteins (5–20nm), are predicted to interact with proteins on 1:1 basis or interact with a subunit of a protein[223]. The opsonization of UNMNPs is largely determined by their surface chemistry such as ligand charge and hydrophobicity. As blood serum is a very complex concoction with thousands of different types of proteins, UNMNPs protected by ligands carrying solely positive or negative charges can bind to serum proteins (or their subunits) with the opposite charge through electrostatic interactions. Whereas UNMNPs with lipophilic ligands can bind to the hydrophobic pocket of some proteins (e.g., albumin) through hydrophobic interactions. Other factors like ligand density[224] and surface charge density[225] that had been identified to affect the protein adsorption of larger nanoparticles remain to be elucidated in the ultrasmall size range. Though opsonized UNMNPs mostly end up in immune organs (liver, spleen, *etc.*) eventually, their specific biodistributions in organ and suborgan level can vary depending on their surface chemistry[226], which are probably due to the different protein-binding scenarios that would influence the nanoparticle-cell interactions *in vivo*[227, 228].

To minimize opsonization and retain the “synthetic identity” of UNMNPs *in vivo*, several surface modification strategies have been established, among which surface coating with antifouling biocompatible polymers, such as the widely used charge-neutral poly(ethylene glycol) (PEG), and zwitterionic molecules like the tripeptide glutathione are the most extensively adopted methods. The antifouling properties of PEGylation arise from the ability of PEG to absorb large amounts of water molecules through ether groups mediated hydrogen-bonding and thus create a water barrier that prevents the adsorption of proteins. Zwitterionization obtains the antifouling function through internally balanced charges and the highly hydrophilic surface created by strong ionic structuring of water[229]. It should be noted that the ligand length of those antifouling coatings also matters, being too short will not provide sufficient protection from opsonization and compromise the physiological stability[230–232] while being too long (e.g., for PEG) will increase the hydrodynamic diameter (HD) of UNMNPs to above KFT (~6nm) and promote MPS uptake[233]. Therefore, to make UNMNPs physiological stable, a highly inert metal (e.g., Au) core and proper-length antifouling ligands that bind to core strongly (e.g., thiols) are preferred. Table 1 summarized the antifouling ligands that were reported to endow UNMNPs with low *in vivo* MPS uptake and efficient renal clearance. Other promising ligands such as polyvinylpyrrolidone (PVP)[234] and zwitterionic carboxybetaine[235], though have not yet been applied to UNMNPs, showed excellent *in vivo* antifouling effect on other types of nanoparticles.

The *in vivo* clearance of UNMNPs is closely associated with their physiological stability. In general, nanoparticles are eliminated via three main pathways: renal, hepatobiliary and through MPS. Antifouling UNMNPs with HD below KFT will be mainly cleared out through kidney into urine. However, the specific renal clearance efficiency and kinetics may vary depending on their surface chemistry properties such as ligand type and surface charge[233, 236]. The other UNMNPs, including those bind to serum proteins and those with HD above KFT, will be eliminated through hepatobiliary route or MPS uptake. Hepatobiliary clearance of nanoparticles involves the interaction of nanoparticles with

hepatocytes via endocytosis or transcytosis and eventually being transported into bile that ends up in feces[237]. In the meantime, MPS such as hepatic Kupffer cells, liver sinusoidal endothelial cells and other tissue macrophages can sequester nanoparticles, particularly those opsonized by proteins. Nanoparticles that undergo hepatobiliary and MPS elimination pathways not only may experience intricate intracellular metabolism during which toxic metabolites can be generated but typically take much longer time to be cleared out (e.g., months to years for MPS uptake), creating concerns of their chronic toxicity[237]. Thus, renal clearance is the preferred clearance pathway for UNMNPs currently. Readers can refer to some excellent reviews for more information on the elimination of nanoparticles *in vivo*[237, 238].

### **Biomedical applications arisen from the *in vivo* stability and clearance properties of UNMNPs**

Though highly stable UNMNPs may seem to be the right choice for biomedical applications, several unique applications actually take advantage of the metastability of some UNMNPs. For example, AgNPs exhibit potent broad-spectrum antibacterial effect which is very promising in tackling the emerging challenges of multidrug-resistant bacteria (or the so-called “superbug”) and one of the main mechanisms of their antimicrobial effect comes from the released Ag<sup>+</sup> ions that interfere the normal metabolism and reproduction of microbes[239, 240]. Ultrasmall AgNPs, due to the high surface to volume ratio and good cell permeability, have been shown to act as better antimicrobial agents compared with their larger counterparts[241–243]. More recently, the synergistic effect was observed by integrating AgNCs and the antibiotic daptomycin[244]. The AgNCs-daptomycin conjugates showed improved antibacterial efficiency over the mere physical mixture of AgNCs and daptomycin (Fig. 6A). UNMNPs that bind to proteins can be exploited as viable tools to modulate the functions of proteins[245, 246]. For instance, ultrasmall anionic AuNPs were able to bind the cationic side chain around the active site of protease  $\alpha$ -chymotrypsin with selectivity and serve as a potent inhibitor of this enzyme[247]. AuNCs used to enhance the enzymatic performance of bilirubin oxidase were also reported[248]. Opsonized UNMNPs usually end up in macrophages *in vivo* and, when coupled with imaging techniques such as computed tomography (CT) or PET, may have the potential for macrophage-related disease imaging[249].

Antifouling UNMNPs have the advantages of reduced *in vivo* non-specific binding and efficient renal clearance (for those HD<6 nm), when combined with their unique physical properties, can lead to some exciting biomedical applications. Ultrasmall luminescent AuNPs with antifouling properties were shown to be able to label proteins without affecting their bioactivities[250, 251], which could be exploited for *in vivo* tracking of proteins with multimodality imaging techniques. Yu et al. demonstrated that glutathione-coated ultrasmall NIR-emitting AuNPs (GS-AuNPs) were excellent nanofluorophores to noninvasively imagine kidney clearance kinetics with significantly improved kidney contrast and imaging-time window over conventional NIR dyes (e.g., Cyanine7, IRDye 800CW) (Fig. 6B)[252]. The noninvasive kidney imaging was made possible by integrating the rapid renal clearance, ultralow skin accumulation (as a result of reduced non-specific binding) and NIR emission of GS-AuNPs. This GSAuNPs enabled fluorescent kidney imaging technique was later

successfully applied to noninvasively differentiate kidney dysfunction stages in a mouse unilateral ureteral obstruction (UUO) model (Fig. 6C)[253]. Combining the efficient renal clearance of GS-AuNPs and the large X-ray absorption cross section of gold atom, Zheng et al. were able to study the *in vivo* transport of renal clearable nanoparticles in both the healthy and injured kidneys with anatomical resolution through X-ray imaging (Fig. 6D) [254]. In addition, the commercialized antifouling 1.9 nm AuNPs (AuroVist™, Nanoprobes Inc.) were proved to be excellent intravenous X-ray imaging contrast agents for the visualization of blood vasculature and urinary system (kidney, ureter, bladder, *etc.*) in mice[255]. The proprietarily formulated AuNPs show a long blood half-life and exhibit significantly enhanced planar X-ray and CT imaging contrasts as compared to the clinical iodine contrast agent iohexol (trade name Omnipaque). Noninvasively monitoring the dynamics of nanoparticle renal clearance via PET imaging was achieved by <sup>64</sup>Cu labeled antifouling ultrasmall AuNPs (Fig. 6E)[256]. Similarly, tracking the renal clearance of nanoparticles through scintigraphy[257] or MRI[258, 259] was also reported by respectively immobilizing other radioisotopes (<sup>99m</sup>Tc, <sup>111</sup>In) or gadolinium onto renal clearable AuNPs.

### Tumor targeting

Nanoparticles are deemed as one of the most promising cancer diagnosis and treatment platforms owing to their targeting capabilities. Nanoparticle-based tumor targeting can be generally divided into two types: passive tumor targeting and active tumor targeting. Passive tumor targeting takes advantage of the tumor's leaky vasculature and poorly functional lymph system so that nanoparticles can cross the tumor blood vessels and accumulate there for prolonged time without being quickly drained away by lymph system (the well-known "EPR" effect). The significantly lowered blood flow velocity within tumor also increases the diffusion of nanoparticles to tumor interstitium[260]. As tumor targeting of nanoparticles through EPR effect can be considered as an accumulative process, nanoparticles with long blood-retention are thus favorable to passively target tumor. It was once believed that tumor targeting via EPR effect was unique to larger nanoparticles with size above KFT as they can escape rapid kidney filtration and circulate in blood for extended time[261]. However, Zheng et al. discovered that ultrasmall luminescent GS-AuNPs could still target tumor passively (~2.3% ID/g at 12h p.i.) through EPR effect, which, coupled with the fast clearance in normal tissues, allowed them to fluorescently detect tumor earlier than that of IRDye 800CW (Fig. 7A)[262]. Though both the GS-AuNPs and the IRDye 800CW share a similar short distribution half-life (~5–6 min) in their two-compartment pharmacokinetics, GS-AuNPs have much longer blood-elimination half-lives (> 8h) than that of IRDye 800CW (< 1h), which is the origin of the observed EPR effect in renal clearable GS-AuNPs. As passive targeting through EPR effect requires the extravasation of nanoparticles from tumor blood vessels, the flow dynamics of nanoparticles within blood vasculature is also critical. Margination dynamics, the lateral motion of nanoparticles towards endothelial walls, is one of the most important factors affecting nanoparticle tumor targeting. Nanoparticles with strong margination effect have higher tendency to extravasate the fenestrated tumor vasculatures and are therefore favorable for tumor targeting. Several factors, such as nanoparticle shape[263], size[264] and density[265], have been identified to significantly affect the margination of larger nanoparticles (>10 nm) in blood circulation and readers can refer to other reviews[266, 267] for detailed account. For UNMNPs, particle density has



been demonstrated to influence their margination effect[96]. Ultrasmall nanoparticles with higher density (AuNPs) were shown to marginate faster to endothelial walls than that of lower density ones (Au-Ag alloy nanoparticles and AgNPs). As blood flow in vasculature is generally laminar, UNMNPs with large margination effect (near the wall of vasculature) would circulate slower than those marginate less (near the center of vasculature), rendering the former a longer blood retention and slower renal clearance that in turn facilitates the tumor targeting. Since margination of nanoparticles in blood vessels is influenced by a number of forces such as hydrodynamic, electrostatic and van der Waals forces[266], other factors like ligand effect are expected to affect the margination of UNMNPs as well through one or more of the above mechanisms. However, exactly how surface ligands influence margination needs further investigations.

Besides passive tumor targeting, UNMNPs can be engineered to actively target tumor by attaching one or multiple types of targeting-moieties to nanoparticle surface. Targeting moieties include small molecules, peptides, oligonucleotides, antibodies as well as other proteins that selectively bind certain membrane receptors overexpressed on tumor cells or tumor vasculatures[268]. Readers are directed to dedicated articles for a comprehensive review of current active targeting ligands and their advantages as well as limitations[269–271]. The merits of active targeting compared to passive one are that it usually offers more targeting selectivity and can facilitate cellular uptake of nanoparticles through specific receptor-mediated internalization[271]. As the active-targeting receptors are located on extravascular tumor cells or the surface of tumor endothelium, those requirements for passive targeting (e.g., long blood-retention, margination) are equally important for active targeting to function well. Moreover, careful design of the UNMNPs surface architectures should be implemented such as ligand type, ligand density and ligand length so that the targeting moieties will not be masked by opsonization, buried by ligands or suffer from too much steric hindrance[271–273]. Of note, successful targeting of tumor cells requires nanoparticles to overcome or bypass a series of biological barriers within tumor microenvironment, including elevated interstitial fluid pressure that hinders the diffusion of nanoparticles, sequestration by non-malignant stromal cells (macrophages, fibroblasts, *etc.*) and extracellular matrix (collagen fibers, proteoglycans, *etc.*) that hampers the penetration of nanoparticles, limiting them in perivascular regions[267, 274]. The spatially and temporally heterogeneous nature of blood perfusion in tumors can lead to the heterogeneity in nanomedicine delivery[260], which may compromise the overall efficacy of cancer treatment. For certain types of nanomedicines that are required to enter specific subcellular compartments such as cytoplasm or nucleus to be effective, they have to escape from endosomes or lysosomes and prevent from being excreted by drug efflux pumps[275].

Compared with larger nanoparticles, UNMNPs not only can reduce normal tissue accumulation and improve tumor targeting specificity (defined as tumor-to-liver ratio for nonrenal clearable nanoparticles; tumor-to-kidney ratio for renal clearable ones)[238], but have advantages in overcoming some of those obstacles for nanoparticle delivery in tumors. The capability of smaller AuNPs to infiltrate deeper into tumor tissues has been observed by Chan et al. over the size range of 15–100 nm[276]. It was further shown that ultrasmall AuNPs (~2nm) have much better permeability both in tumor organ level and cellular level compared to their larger counterparts (~15nm), exemplifying the advantages of UNMNPs in

tumor penetration and accumulation[277]. For example, compared to that of 18 nm AuNPs, ultrasmall (~3 nm) AuNPs shows much higher targeting efficiency and targeting specificity for glioblastoma, the most malignant orthotopic brain tumor that is also extremely challenging for nanoparticle delivery because of the blood-brain barrier and blood-tumor barrier[278]. Size-dependent nucleus entry was also observed and ultrasmall AuNPs (~2nm) could enter the tumor cell nucleus whereas larger ones (10–16 nm) were only confined in cytoplasm[279]. The superior permeability of UNMNPs makes them promising candidates to serve as delivery agents for cancer therapeutics.

The tumor targeting efficiency of renal clearable UNMNPs can be further improved through proper engineering of their surface chemistries or metal cores. One apparent way is to integrate both passive targeting and active targeting by appropriately attaching active-targeting ligands onto the surface of UNMNPs. In this way, the targeting enhancement mainly comes from stronger receptor-mediated nanoparticle-cell interactions and subsequent endocytosis, leading to the increased retention of UNMNPs at tumor sites. For example, AuNCs conjugated with folic acid, a small molecule targeting ligand, were shown to have improved tumor targeting efficiency compared with AuNCs alone by several groups[280–282]. However, extra attention should be paid when performing surface modification with targeting ligands otherwise the effectiveness of active targeting could be counterbalanced or even outweighed by the compromised *in vivo* stability (e.g., rapid opsonization, increased MPS uptake) of UNMNPs. Another method is to extend the blood-retention time of UNMNPs by surface coating with PEG molecules of proper length and density[233, 283]. Zheng et al. conducted a head-to-head comparison of PEG-coated ultrasmall AuNPs (PEG-AuNPs) with ultrasmall GS-AuNPs sharing almost identical core size and high physiological stability (Fig. 7B)[233]. They found that PEG-AuNPs have much higher tumor targeting efficiency as compared to that of GS-AuNPs (8.3% vs. 2.3% ID/g at 12h p.i.) though both of them can be eventually eliminated via urine with low accumulation in MPS. The high passive targeting efficiency of PEG-AuNPs fundamentally results from their increased retention time and concentration in blood, which is also supported by the slow normal tissue clearance and renal clearance of PEG-AuNPs. It is noteworthy that PEG-AuNPs are cleared from tumor faster than that of GS-AuNPs, which is very likely due to the lower cell uptake efficiency of AuNPs coated with PEG than that coated with zwitterionic ligands (e.g., GSH) as reported elsewhere[284–286]. The effects of PEGylation in slowing the renal clearance and increasing the blood-retention as well as tumor-targeting of ultrasmall AuNPs were also observed by Liang et al.[283]. However, the exact origin of these PEGylation effects on UNMNPs *in vivo* behavior requires further study. In addition, the targeting efficiency of UNMNPs could be enhanced by taking advantage of some unique features of solid tumors such as the acidic tumor microenvironment. Zheng et al. synthesized ultrasmall glutathione/cysteamine dual-ligand coated AuNPs (GC-AuNPs) that exhibit strong cell membrane binding at acidic pH while minimal binding at normal physiological pH (7.4)[287]. They found that the acidity-targeting GC-AuNPs indeed could improve the targeting efficiency of more acidic tumors in a specific time window (Fig. 7C)[288].

Besides surface engineering, the metal cores of UNMNPs are also relevant to their tumor targeting abilities. As mentioned previously, the density of metal cores could affect margination of UNMNPs in vasculatures and UNMNPs with higher core density are

preferred for better targeting efficiency[96]. Moreover, for nanoparticles in the ultrasmall size range, their subtle variations may seem irrelevant to their tumor targeting, but recently it was found that when the size of AuNPs decreases to sub-nm regime their tumor-targeting efficiency increases rapidly with descending sizes (from ~2% ID/g of Au<sub>25</sub>(SG)<sub>18</sub> to ~8% ID/g of Au<sub>10-11</sub>(SG)<sub>10-11</sub>) [63]. This size-dependent tumor targeting of sub-nm AuNCs originates from the fact that smaller AuNCs are retained by kidney glomeruli to a greater extent than that of larger AuNCs, which significantly prolongs the blood-retention of smaller AuNCs and increases their passive tumor targeting through EPR effect (Fig. 7D). Finally, it should be mentioned that tumor targeting efficiency of UNMNPs is influenced by both tumor type and tumor size as different type and stage of tumors can possess distinct tumor microenvironment that affects the accumulation and retention of nanoparticles.

### Biomedical applications arisen from the tumor targeting properties of UNMNPs

Integrating the tumor targeting capability of UNMNPs and their other physical as well as physiological properties has been yielding numerous biomedical applications. Ultrasmall luminescent AuNPs enabled *in vivo* fluorescence tumor imaging has been widely reported based on either passive[75, 262] or active[280, 282] targeting methods. When incorporating with radioisotopes or paramagnetic elements, ultrasmall AuNPs are able to detect tumors via nuclear medicine imaging[100, 124] or MRI[289, 290] that are free from tissue penetration limitations (Fig. 8A). As gold (Z=79) and platinum (Z=78) have large atomic numbers and are able to efficiently absorb ionizing radiations (X-rays, Gamma rays, *etc.*) and generate secondary radiations to amplify the local radiation exposure, ultrasmall small AuNPs[67, 291–293] and PtNPs[294, 295] can serve as radiosensitizers to enhance cancer radiation therapy. It is worth pointing out that by combining the radiosensitization effect of gold and size-dependent passive tumor targeting efficiency of sub-nm AuNCs, Xie et al. demonstrated the use of Au<sub>10-12</sub>(SG)<sub>10-12</sub> as a new class of radiosensitizers for high tumor specificity and cancer radiotherapy (Fig. 8B)[67]. UNMNPs are excellent carriers for cancer therapeutic agents thanks to the ultrasmall sizes that endow them with high tumor permeability. Li et al. reported a ultrasmall AuNCs-based cancer theranostic platform by conjugating cisplatin prodrug and active-targeting ligand folic acid onto NIR-emitting AuNCs[296]. *In vivo* study proved that this new nanoplatform could improve therapeutic efficacy for both primary and metastasis cancers (Fig. 8C). Similarly, photosensitizer incorporated luminescent AuNCs have been applied in fluorescence-guided photodynamic therapy and exhibited efficient tumor penetration and destruction ability (Fig. 8D)[281, 297]. The nuclear pore complex that acts as a gateway for nucleocytoplasmic exchange is about 6–10nm in diameter, which allows ultrasmall nanoparticles to enter nucleus more easily than larger ones through passive diffusion[298]. Several *in vitro* and *in vivo* studies have shown that ultrasmall AuNPs are promising vehicles to deliver therapeutic agents, such as chemotherapy drug[299–301], antibody[302] and gene[279, 303], to the nucleus of cancer cells.

### Toxicity

Understanding the toxicity profiles of UNMNPs and their affecting factors are indispensable for the successful clinical translation. Though numerous studies have been performed to elucidate the relationship between the physical/chemical properties of nanoparticles and the corresponding toxicity effects, most of them focused on larger nanoparticles (>3 nm). Since

many physical and physiological properties of nanoparticles are well known to be size-dependent, the toxicity of UNMNPs may not follow the exact same rules as that of their larger counterparts. Moreover, majority of the toxicity studies were done at *in vitro* cellular level, which, although is helpful to gain some insights into the toxicity mechanism, oversimplified the bio-nano interactions they experienced *in vivo*. In a complex, dynamic, multicellular *in vivo* environment, the physical and physiological properties of UNMNPs are subject to modification or metabolism by many factors such as opsonization and fast circulation, leading to the possible inconsistency between *in vitro* and *in vivo* results[304]. In this part, we will mainly summarize the toxicity studies conducted using UNMNPs and compare the results with that from larger ones, with an emphasis on *in vivo* studies.

Both core and surface chemistry were shown to affect the toxicity of UNMNPs. It was demonstrated both in mice[305] and zebrafish[306] that ultrasmall AgNPs exhibit higher toxicity than that of ultrasmall AuNPs, which is in agreement with other *in vitro*[307, 308] and *in vivo*[309] studies conducted using larger nanoparticles, proving that the core chemical composition of UNMNPs plays an important role in affecting their toxicity. The toxicity of AgNPs has been linked to their relatively poor physiological stability and bio-inertness, which would lead to the gradual release of Ag<sup>+</sup> ions and generation of oxidative stress after entering cells. Surface coating AgNPs with proper ligands such as PEG or albumin is able to improve the physiological stability of AgNPs and reduce their toxicity[310]. Surface chemistry, such as ligand type and surface charge, can have significant impact on the biodistribution, elimination and cellular interaction of UNMNPs, and thus profoundly affects their toxicity. For example, 1.4nm phosphine-stabilized AuNPs could irreversibly block membrane ion channels and show high cytotoxicity *in vitro*, whereas AuNPs stabilized by strong-binding thiol ligands with the same size are not cytotoxic, highlighting the influence of ligand type in modulating UNMNPs toxicity[156]. In addition, both phosphine- and thiol-stabilized 1.4nm AuNPs cannot block the ion channel *in vivo* after intravenous injection because of rapid binding of phosphine-stabilized AuNPs to serum proteins that prevents the direct interaction of AuNPs with ion channels. In general, positively charged nanoparticles are less biocompatible than negative charged or neutral ones[311–313]. Ultrasmall thiolated AuNPs with cationic ligands (quaternary amines) were observed to be much more toxic than that with anionic ligands (carboxylic groups) *in vitro*[314], which is due to the fact that cationic nanoparticles could bind to cell membrane through strong electrostatic interactions that destabilize the plasma membrane and compromise its integrity. The degree of membrane disruption and cytotoxicity as well as cell internalization route are strongly influenced by the surface charge density of ultrasmall AuNPs[315]. While under the *in vivo* circumstance, highly positively charged UNMNPs will first bind to abundant negatively charged serum proteins after intravenous administration and the protein-nanoparticle complex usually will have much less membrane adsorption compared with that of bare nanoparticles[316, 317] and will be rapidly sequestered by MPS, thus reducing the nanoparticle exposure to other tissues and minimizing associated toxicity.

However, even for the most “biocompatible” AuNPs, long-term accumulation in MPS could lead to adverse effects like inflammatory immune responses and cellular apoptosis in organs such as liver and spleen[318], possibly due to release of toxic metal ions and oxidative stress induced by the intracellular degradation and metabolism of noble metal nanoparticles[319,

320]. Therefore, nanoparticles should be completely eliminated from the body in a reasonable time period to minimize health hazard, which is also the guideline of U.S. Food and Drug Administration (FDA) for pharmaceutical drugs or contrast agents. Since efficient hepatobiliary clearance of inorganic nanoparticles is hard to realize at present stage, highly renal clearable UNMNPs are thus preferred in order to reduce toxicity risk. The toxicity of renal clearable glutathione coated ultrasmall (~2nm) AuNPs (GS-AuNPs) were systematically evaluated both in mice and monkeys recently[321]. No adverse effect was observed within 14 days in CD-1 mice even at the highest injection dose (1059mg/kg), which is higher than the maximal tolerated dose (450mg/kg) of highly biocompatible silica nanoparticles in CD-1 mice, and also no side effect occurred to cynomolgus monkeys within 90 days after receiving an injection dose of 250mg/kg GS-AuNPs. The superior biocompatibility of GS-AuNPs originates from the dose-dependent transport of nanoparticles in blood vessels and at higher doses (>15mg/kg) GS-AuNPs are confined in the blood vessels with reduced percentage of margination and diffusion into background tissues as compared with that of low doses (Fig. 9A and B). The dose-dependent *in vivo* transport leads to shortened blood-retention and expedited renal clearance of GS-AuNPs when injected at high doses, which can significantly reduce the accumulation of GS-AuNPs in normal tissues and reduce their toxicity.

### Biomedical applications arisen from the toxicity properties of UNMNPs

Control the cellular toxicity of UNMNPs is a prerequisite for their applications in live cell sensing and tracking. Lipoic acid stabilized ultrasmall luminescent AuNPs (LA-AuNPs) were reported to have minimal cellular toxicity and were incorporated into multiple endothelial cells for long-term (> 20 days) fluorescence *in vivo* living cell tracking (Fig. 9C) [322]. It was shown that the LA-AuNPs loaded endothelial cells had much better viability compared to that loaded with quantum dots and exhibited intact cellular function/expression profiles such as angiogenesis, vasodilation, migration, adhesion and growth as revealed by *in vivo* and *in vitro* fluorescent imaging. The low cellular toxicity of LA-AuNPs coupled with their intrinsic NIR-emitting properties also enabled researchers to study their cellular uptake mechanism and intracellular fate following internalization[323]. Jiang et al. recently reported that quaternary ammonium/glutathione co-capped ultrasmall AuNCs could serve as novel potent antibiotics to target and combat multidrug-resistant (MDR) bacteria infection *in vivo* using several mouse models[324]. The extraordinary antibiotic activity of these AuNCs towards MDR bacteria was thought to result from a synergistic effect, including cationic surface chemistry induced cell membrane disruption, size-related catalytic generation of oxidative stress and disturbance of intracellular metabolic pathways. Although in many cases nanoparticle-induced immune response is regarded as side effect since it often leads to inflammation and cellular death, at certain conditions UNMNPs could be used to modulate immune cells and stimulate beneficial immune response for combating diseases. *In vitro* experiments demonstrated that ultrasmall zwitterionic AuNPs were efficiently taken up by human dendritic cells (DCs) with low cytotoxicity and able to induce the maturation of DCs for antigen presentation while suppressing inflammatory responses (Fig. 9D), which was in distinct contrast to larger AuNPs (~12nm) that only elicited inflammation[285]. Thus, these ultrasmall zwitterionic AuNPs can serve as promising immune adjuvant or suitable platform for vaccine displays. *In vivo* application of ultrasmall AuNCs as delivery agents to co-

deliver both antigens and immune adjuvants to antigen presenting cells (APCs) was reported by Qu et al.[325]. The new vaccine system was proved to be highly biocompatible and exhibited much higher immunostimulatory activity compared to the physical mixture of antigens and adjuvants.

## Conclusion and Perspective

In summary, we briefly summarized the breakthroughs of UNMNPs over the past decade in terms of the preparation (precisely-controlled synthesis, doping and alloying), understanding of their physical properties (structures and optical characteristics) as well as physiological properties (*in vivo* stability, clearance, tumor targeting and toxicity). The related biomedical applications enabled by these breakthroughs were also demonstrated. Compared with their large counterparts, UNMNPs do offer many uniqueness and advantages that can help to tackle some of the current challenges in nanomedicine. UNMNPs can be designed to enable efficient renal clearance and avoid long-term accumulation in MPS organs (liver, spleen, etc.), which not only reduce possible interference with subsequent imaging or therapy practices but also minimize potential side effects, a prerequisite for successful clinical translation. Besides, many unique properties evolve only at the ultrasmall size scale. For instance, due to synergistic mechanism, much stronger antibiotic efficacy was usually observed in UNMNPs as compared to that of their larger ones, which represents a promising tactic to battle drug-resistant bacterial infection, an increasingly serious problem in the 21<sup>st</sup> century. These unique features of UNMNPs have already made significant contributions to expediting both the fundamental understandings and practical applications of nanomedicine.

While significant progresses have been made, some important questions and challenges remain to be addressed in order to accelerate the clinical translation of UNMNPs and maximize their potential. For example, as to the precisely-controlled preparation of UNMNPs, currently most of the well-defined nanoparticles are organic soluble which limited their biomedical applications. More effort should be devoted to establishing scalable synthetic routes to atomic precise, stable, water soluble UNMNPs with different sizes, especially those protected by anti-biofouling ligands. In addition, how to precisely control the surface functionalization on these atomic precise nanoparticles is another important direction. Since in many cases extra ligands, like active-targeting molecules, drugs and photosensitizers, are conjugated onto nanoparticles, their configuration (e.g., quantity, distribution, conformation) on nanoparticle will inevitably affect the bio-nano interactions and thus the efficacy of nanomedicine eventually. The realization of atomic precise nanoparticles makes it possible to precisely control their surface modification, which not only is significant for the optimization of nanomedicine but also ensures a high reproducibility that is crucial for clinical translation. Though chiral UNMNPs have been widely reported during the past decade, the exploitation of their biomedical application is still in its infant stage. As the physical dimensions of UNMNPs are comparable to many important biomolecules (proteins, nucleic acids, etc.), of which interactions are known to be chiral selective, it is thus interesting to investigate how different chiral UNMNPs interact with those natural biomolecules and how these chiral bio-nano interactions could bring forth new analytical tools or therapeutic drugs. Moreover, majority of the current UNMNPs-based biomedical applications are focused on cancer, whereas how to apply UNMNPs to solve

other health problems deserves more attention. Considering that a number of inflammatory and cardiovascular diseases share many common characteristics with that of cancer such as angiogenesis and increased endothelial permeability, the high permeability and low non-specific accumulation of UNMNPs can also be helpful for the targeting and delivering of therapeutics to the lesion sites of those diseases with reduced side effects. In addition, mounting evidence has revealed that some noble metals, like Au, could have intrinsic anti-inflammation effect[326, 327], which might render UNMNPs of those metals useful for inflammation-associated illnesses such as various autoimmune diseases and cardiovascular diseases like atherosclerosis.

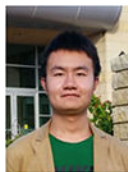
For the fundamental understanding of UNMNPs physiological behavior, many aspects are still not thoroughly clear. For instance, how UNMNPs are metabolized step by step when they are internalized by cells (e.g., macrophage, endothelium, hepatocytes) and how they are cleared out remain to be clarified. The elucidation of UNMNPs metabolism pathways contributes to a more complete understanding of their toxicity and helps to design more efficient nanomedicines with good biocompatibility. UNMNPs with well-defined composition and structure could serve as excellent models to study the metabolism of nanoparticles. The *in vivo* transport of UNMNPs is also critical and deserves more investigations. After introducing UNMNPs to the body, how they interact with different compartments and cells in each organ/tissue along their transporting route determines the biodistribution and potential toxicity of UNMNPs. For example, as urinary clearance is the major elimination pathway for many renal clearable UNMNPs, the interaction of UNMNPs with different cells (endothelial cells, proximal tubular cells, distal tubular cells, *etc.*) in kidney and their affecting factors should be evaluated. Strategies to manipulate these bio-nano interactions shall be developed afterwards and translate our basic understandings into new practical applications to tackle biomedical challenges.

Overall, UNMNPs have many unique advantages and exhibit great potential in biomedical research. While challenges do exist, tremendous opportunities and possibilities are also awaiting us. With collective efforts from the growing number of researchers who joined the field of UNMNPs, we anticipate that UNMNPs will play an even more important role in the near future for both the basic and applied biomedical science.

## Acknowledgement

J.Z. acknowledges the financial support from National Institutes of Health (NIH) (1R01DK103363), Cancer Prevention Research Instituted of Texas (CPRIT) (RP140544, RP120588) and the start-up fund from the University of Texas at Dallas.

## Biographies



**Xingya Jiang** received his BS in Applied Chemistry from Beijing Institute of Technology in 2014 and joined Dr. Jie Zheng's group at the University of Texas at Dallas the same year as a graduate student. He is now a PhD candidate with research interests spanning from the design and synthesis of nanomedicines to their novel biomedical applications.



**Bujie Du** is a graduate student at the Chemistry & Biochemistry department of the University of Texas at Dallas. She received her BS in Chemistry from Beijing Institute of Technology. In fall 2014, she started her graduate studies with Prof. Jie Zheng at UT Dallas, focusing on the fundamental studies of nano-bio interactions of engineered nanoparticles.



**Yingyu Huang** was born in 1993 in Hubei China. He received his BS in Chemistry in 2015 from Beijing Institute of Technology. Currently he is pursuing his PhD degree under the supervision of Dr. Jie Zheng at the University of Texas at Dallas. His current research focus is on the synthesis, properties and biomedical applications of luminescent gold nanoparticles.



**Dr. Jie Zheng** received his PhD degree from Georgia Institute of Technology in 2005. After three-years postdoctoral research at Harvard University, he joined the chemistry department at the University of Texas at Dallas as an assistant professor. He is now the associate professor of Chemistry & Biochemistry at the University of Texas at Dallas and also the adjunct associate professor of Urology at the University of Texas Southwestern Medical Center. His research interests focus on luminescent metal nanostructures and understanding of nano-bio interactions and transport at both *in vitro* and *in vivo* levels.

## References

- [1]. Ozin GA, Huber H, Inorg. Chem, 17 (1978) 155–163.
- [2]. Faraday M, Philos. Trans. R. Soc. London, 147 (1857) 145–181.
- [3]. Jarrell M, Gates B, Nicholson E, J. Am. Chem. Soc, 100 (1978) 5727–5732.
- [4]. Mason M, Physical review B, 27 (1983) 748.



- [5]. Pierantozzi R, McQuade KJ, Gates BC, Wolf M, Knoezinger H, Ruhmann W, *J. Am. Chem. Soc.*, 101 (1979) 5436–5438.
- [6]. Hamilton J, Baetzold R, *Science*, 205 (1979) 1213–1220. [PubMed: 17750133]
- [7]. Valden M, Lai X, Goodman DW, *Science*, 281 (1998) 1647–1650. [PubMed: 9733505]
- [8]. Peyser LA, Vinson AE, Bartko AP, Dickson RM, *Science*, 291 (2001) 103–106. [PubMed: 11141556]
- [9]. Zhang L, Wang E, *Nano Today*, 9 (2014) 132–157.
- [10]. Shang L, Dong S, Nienhaus GU, *Nano Today*, 6 (2011) 401–418.
- [11]. Tan X, Jin R, *Wiley Interdisciplinary Reviews: Nanomedicine and Nanobiotechnology*, 5 (2013) 569–581. [PubMed: 23939885]
- [12]. Kim BH, Hackett MJ, Park J, Hyeon T, *Chem. Mater.*, 26 (2013) 59–71.
- [13]. Zhu M, Lanni E, Garg N, Bier ME, Jin R, *J. Am. Chem. Soc.*, 130 (2008) 1138–1139. [PubMed: 18183983]
- [14]. Wu Z, Suhan J, Jin R, *J. Mater. Chem.*, 19 (2009) 622–626.
- [15]. Toikkanen O, Ruiz V, Rönholm G, Kalkkinen N, Liljeroth P, Quinn BM, *J. Am. Chem. Soc.*, 130 (2008) 11049–11055. [PubMed: 18652456]
- [16]. Qian H, Zhu Y, Jin R, *Acs Nano*, 3 (2009) 3795–3803. [PubMed: 19860401]
- [17]. Zeng C, Chen Y, Li G, Jin R, *Chem. Mater.*, 26 (2014) 2635–2641.
- [18]. Li G, Zeng C, Jin R, *J. Am. Chem. Soc.*, 136 (2014) 3673–3679. [PubMed: 24568535]
- [19]. Qian H, Jin R, *Nano Lett.*, 9 (2009) 4083–4087. [PubMed: 19995083]
- [20]. Qian H, Zhu Y, Jin R, *Proceedings of the National Academy of Sciences*, 109 (2012) 696–700.
- [21]. Yu Y, Chen X, Yao Q, Yu Y, Yan N, Xie J, *Chem. Mater.*, 25 (2013) 946–952.
- [22]. Yao Q, Yu Y, Yuan X, Yu Y, Xie J, Lee JY, *Small*, 9 (2013) 2696–2701. [PubMed: 23447552]
- [23]. Ghosh A, Udayabhaskararao T, Pradeep T, *The Journal of Physical Chemistry Letters*, 3 (2012) 1997–2002.
- [24]. Joshi CP, Bootharaju MS, Bakr OM, *The journal of physical chemistry letters*, 6 (2015) 3023–3035. [PubMed: 26267198]
- [25]. Desireddy A, Conn BE, Guo J, Yoon B, Barnett RN, Monahan BM, Kirschbaum K, Griffith WP, Whetten RL, Landman U, *Nature*, 501 (2013) 399. [PubMed: 24005327]
- [26]. Cathcart N, Kitaev V, *The Journal of Physical Chemistry C*, 114 (2010) 16010–16017.
- [27]. Tanaka SI, Miyazaki J, Tiwari DK, Jin T, Inouye Y, *Angew. Chem.*, 123 (2011) 451–455.
- [28]. Imaoka T, Kitazawa H, Chun W-J, Omura S, Albrecht K, Yamamoto K, *J. Am. Chem. Soc.*, 135 (2013) 13089–13095. [PubMed: 23902457]
- [29]. Erickson JD, Mednikov EG, Ivanov SA, Dahl LF, *J. Am. Chem. Soc.*, 138 (2016) 1502–1505. [PubMed: 26790717]
- [30]. Mednikov EG, Dahl LF, *Philosophical Transactions of the Royal Society of London A: Mathematical, Physical and Engineering Sciences*, 368 (2010) 1301–1332.
- [31]. Yamamoto H, Maity P, Takahata R, Yamazoe S, Koyasu K, Kurashige W, Negishi Y, Tsukuda T, *The Journal of Physical Chemistry C*, 121 (2017) 10936–10941.
- [32]. Udayabhaskararao T, Pradeep T, *The journal of physical chemistry letters*, 4 (2013) 1553–1564. [PubMed: 26282314]
- [33]. Lu Y, Chen W, *Chem. Soc. Rev.*, 41 (2012) 3594–3623. [PubMed: 22441327]
- [34]. Zheng K, Yuan X, Goswami N, Zhang Q, Xie J, *RSC Advances*, 4 (2014) 60581–60596.
- [35]. Chakraborty I, Pradeep T, *Chem. Rev.* (2017).
- [36]. Van der Velden J, Vollenbroek F, Bour J, Beurskens P, Smits J, Bosnian W, *Recl. Trav. Chim. Pays-Bas*, 100 (1981) 148–152.
- [37]. van der Velden JW, Bour JJ, Bosman WP, Noordik JH, *J. Chem. Soc., Chem. Commun.* (1981) 1218–1219.
- [38]. Briant CE, Hall KP, Wheeler AC, Mingos DMP, *J. Chem. Soc., Chem. Commun.* (1984) 248–250.
- [39]. Bellon P, Manassero M, Sansoni M, *J. Chem. Soc., Dalton Trans.* (1972) 1481–1487.

- [40]. Schmid G, Pfeil R, Boese R, Bandermann F, Meyer S, Calis G, van der Velden JW, Eur. J. Inorg. Chem, 114 (1981) 3634–3642.
- [41]. Schmid G, Chem. Soc. Rev, 37 (2008) 1909–1930. [PubMed: 18762839]
- [42]. Schmid G, Giebel U, Huster W, Schwenk A, Inorg. Chim. Acta, 85 (1984) 97–102.
- [43]. Schmid G, Morun B, Malm JO, Angew. Chem. Int. Ed, 28 (1989) 778–780.
- [44]. Schmid G, Klein N, Morun B, Lehnert A, Malm J-O, Pure Appl. Chem, 62 (1990) 1175–1177.
- [45]. Jadzinsky PD, Calero G, Ackerson CJ, Bushnell DA, Kornberg RD, Science, 318 (2007) 430–433. [PubMed: 17947577]
- [46]. Schaaff TG, Knight G, Shafiqullin MN, Borkman RF, Whetten RL, The Journal of Physical Chemistry B, 102 (1998) 10643–10646.
- [47]. Schaaff TG, Whetten RL, The Journal of Physical Chemistry B, 104 (2000) 2630–2641.
- [48]. Zheng J, Petty JT, Dickson RM, J. Am. Chem. Soc, 125 (2003) 7780–7781. [PubMed: 12822978]
- [49]. Xie J, Zheng Y, Ying JY, J. Am. Chem. Soc, 131 (2009) 888–889. [PubMed: 19123810]
- [50]. Le Guével X, Daum N, Schneider M, Nanotechnology, 22 (2011) 275103. [PubMed: 21613679]
- [51]. Baksi A, Xavier PL, Chaudhari K, Goswami N, Pal S, Pradeep T, Nanoscale, 5 (2013) 2009–2016. [PubMed: 23369925]
- [52]. Petty JT, Zheng J, Hud NV, Dickson RM, J. Am. Chem. Soc, 126 (2004) 5207–5212. [PubMed: 15099104]
- [53]. Vosch T, Antoku Y, Hsiang J-C, Richards CI, Gonzalez JI, Dickson RM, Proceedings of the National Academy of Sciences, 104 (2007) 12616–12621.
- [54]. Zheng J, Zhang C, Dickson RM, Phys. Rev. Lett, 93 (2004) 077402. [PubMed: 15324277]
- [55]. Habeeb Muhammed MA, Ramesh S, Sinha SS, Pal SK, Pradeep T, Nano Research, 1 (2008) 333–340.
- [56]. Muhammed MAH, Verma PK, Pal SK, Kumar R, Paul S, Omkumar RV, Pradeep T, Chemistry-a European Journal, 15 (2009) 10110–10120.
- [57]. Zeng C, Qian H, Li T, Li G, Rosi NL, Yoon B, Barnett RN, Whetten RL, Landman U, Jin R, Angew. Chem, 124 (2012) 13291–13295.
- [58]. Luo Z, Nachammai V, Zhang B, Yan N, Leong DT, D.-e. Jiang, J. Xie, J. Am. Chem. Soc, 136 (2014) 10577–10580. [PubMed: 25014336]
- [59]. Liu C, Pei Y, Sun H, Ma J, J. Am. Chem. Soc, 137 (2015) 15809–15816. [PubMed: 26605978]
- [60]. Liu C, Li G, Pang G, Jin R, RSC Advances, 3 (2013) 9778–9784.
- [61]. Barngrover BM, Aikens CM, J. Am. Chem. Soc, 134 (2012) 12590–12595. [PubMed: 22827488]
- [62]. Yao Q, Yuan X, Fung V, Yu Y, Leong DT, Jiang D.-e., Xie J, Nature Communications, 8 (2017).
- [63]. Du B, Jiang X, Das A, Zhou Q, Yu M, Jin R, Zheng J, Nature nanotechnology, (2017).
- [64]. Wong OA, Hansen RJ, Ni TW, Heinecke CL, Compel WS, Gustafson DL, Ackerson CJ, Nanoscale, 5 (2013) 10525–10533. [PubMed: 24057086]
- [65]. Tay CY, Yu Y, Setyawati MI, Xie J, Leong DT, Nano Research, 7 (2014) 805–815.
- [66]. Kawasaki H, Kumar S, Li G, Zeng C, Kauffman DR, Yoshimoto J, Iwasaki Y, Jin R, Chem. Mater, 26 (2014) 2777–2788.
- [67]. Zhang XD, Luo Z, Chen J, Shen X, Song S, Sun Y, Fan S, Fan F, Leong DT, Xie J, Adv. Mater, 26 (2014) 4565–4568. [PubMed: 24817169]
- [68]. Pan Y, Neuss S, Leifert A, Fischler M, Wen F, Simon U, Schmid G, Brandau W, Jahnen-Dechent W, Small, 3 (2007) 1941–1949. [PubMed: 17963284]
- [69]. Zheng K, Setyawati MI, Leong DT, Xie J, ACS nano, (2017).
- [70]. Pyo K, Ly NH, Yoon SY, Shen Y, Choi SY, Lee SY, Joo SW, Lee D, Advanced Healthcare Materials, (2017).
- [71]. Wu Z, Wang M, Yang J, Zheng X, Cai W, Meng G, Qian H, Wang H, Jin R, Small, 8 (2012) 2028–2035. [PubMed: 22488747]
- [72]. Ghosh S, Anand U, Mukherjee S, Anal. Chem, 86 (2014) 3188–3194. [PubMed: 24528116]
- [73]. Yang J, Xia N, Wang X, Liu X, Xu A, Wu Z, Luo Z, Nanoscale, 7 (2015) 18464–18470. [PubMed: 26509471]

- [74]. Tanaka S.-i., Aoki K, Muratsugu A, Ishitobi H, Jin T, Inouye Y, *Optical Materials Express*, 3 (2013) 157–165.
- [75]. Wu X, He X, Wang K, Xie C, Zhou B, Qing Z, *Nanoscale*, 2 (2010) 2244–2249. [PubMed: 20835443]
- [76]. Wang M, Wu Z, Yang J, Wang G, Wang H, Cai W, *Nanoscale*, 4 (2012) 4087–4090. [PubMed: 22522406]
- [77]. Qu X, Li Y, Li L, Wang Y, Liang J, *Journal of Nanomaterials*, 2015 (2015) 4.
- [78]. Yuan X, Luo Z, Yu Y, Yao Q, Xie J, *Chemistry–An Asian Journal*, 8 (2013) 858–871.
- [79]. Chen L-Y, Wang C-W, Yuan Z, Chang H-T, *Anal. Chem.*, 87 (2014) 216–229. [PubMed: 25275676]
- [80]. Patel SA, Richards CI, Hsiang J-C, Dickson RM, *J. Am. Chem. Soc.*, 130 (2008) 11602. [PubMed: 18686957]
- [81]. Yau SH, Abeyasinghe N, Orr M, Upton L, Varnavski O, Werner JH, Yeh H-C, Sharma J, Shreve AP, Martinez JS, *Nanoscale*, 4 (2012) 4247–4254. [PubMed: 22692295]
- [82]. Ramakrishna G, Varnavski O, Kim J, Lee D, Goodson T, *J. Am. Chem. Soc.*, 130 (2008) 5032–5033. [PubMed: 18357982]
- [83]. Oh E, Fatemi FK, Currie M, Delehanty JB, Pons T, Fragola A, Lévêque-Fort S, Goswami R, Susumu K, Huston AL, *Particle & Particle Systems Characterization*, 30 (2013) 453–466.
- [84]. Abeyasinghe N, Kumar S, Sun K, Mansfield JF, Jin R, Goodson T III, *J. Am. Chem. Soc.*, 138 (2016) 16299–16307. [PubMed: 27957846]
- [85]. Wang T, Wang D, Padelford JW, Jiang J, Wang G, *J. Am. Chem. Soc.*, 138 (2016) 6380–6383. [PubMed: 27172252]
- [86]. Fang Y-M, Song J, Li J, Wang Y-W, Yang H-H, Sun J-J, Chen G-N, *Chem. Commun.*, 47 (2011) 2369–2371.
- [87]. Swanick KN, Hesari M, Workentin MS, Ding Z, *J. Am. Chem. Soc.*, 134 (2012) 15205–15208. [PubMed: 22928664]
- [88]. Hesari M, Workentin MS, Ding Z, *ACS nano*, 8 (2014) 8543–8553. [PubMed: 25088234]
- [89]. Hesari M, Ding Z, Workentin MS, *Organometallics*, 33 (2014) 4888–4892.
- [90]. Li L, Liu H, Shen Y, Zhang J, Zhu J-J, *Anal. Chem.*, 83 (2011) 661–665. [PubMed: 21226463]
- [91]. Hesari M, Ding Z, *Acc. Chem. Res.*, 50 (2017) 218–230. [PubMed: 28080028]
- [92]. Díez I, Pusa M, Kulmala S, Jiang H, Walther A, Goldmann AS, Müller AH, Ikkala O, Ras RH, *Angew. Chem. Int. Ed.*, 48 (2009) 2122–2125.
- [93]. Feng L, Wu L, Xing F, Hu L, Ren J, Qu X, *Biosens. Bioelectron.*, 98 (2017) 378–385. [PubMed: 28709087]
- [94]. Ferrando R, Jellinek J, Johnston RL, *Chem. Rev.*, 108 (2008) 845–910. [PubMed: 18335972]
- [95]. Jin R, Nobusada K, *Nano Research*, 7 (2014) 285.
- [96]. Tang S, Peng C, Xu J, Du B, Wang Q, Vinluan RD, Yu M, Kim MJ, Zheng J, *Angew. Chem.*, 128 (2016) 16273–16277.
- [97]. Kumara C, Dass A, *Nanoscale*, 3 (2011) 3064–3067. [PubMed: 21750816]
- [98]. Kumara C, Dass A, *Nanoscale*, 4 (2012) 4084–4086. [PubMed: 22370910]
- [99]. Wu M-L, Chen D-H, Huang T-C, *Langmuir*, 17 (2001) 3877–3883.
- [100]. Zhao Y, Detering L, Sultan D, Cooper ML, You M, Cho S, Meier SL, Luehmann H, Sun G, Rettig M, *ACS nano*, 10 (2016) 5959–5970. [PubMed: 27159079]
- [101]. Zhao Y, Sultan D, Detering L, Luehmann H, Liu Y, *Nanoscale*, 6 (2014) 13501–13509. [PubMed: 25266128]
- [102]. Gottlieb E, Qian H, Jin R, *Chemistry-A European Journal*, 19 (2013) 4238–4243.
- [103]. Kauffman DR, Alfonso D, Matraga C, Qian H, Jin R, (2013).
- [104]. Negishi Y, Munakata K, Ohgake W, Nobusada K, *The journal of physical chemistry letters*, 3 (2012) 2209–2214. [PubMed: 26295772]
- [105]. Qian H, Jiang D.-e., Li G, Gayathri C, Das A, Gil RR, Jin R, *J. Am. Chem. Soc.*, 134 (2012) 16159–16162. [PubMed: 22992034]
- [106]. Christensen SL, MacDonald MA, Chatt A, Zhang P, Qian H, Jin R, (2012).

- [107]. Negishi Y, Igarashi K, Munakata K, Ohgake W, Nobusada K, Chem. Commun, 48 (2012) 660–662.
- [108]. QIAN H, BARRY E, Zhu Y, JIN R, Acta Physico-Chimica Sinica, 27 (2011) 513–519.
- [109]. Biltek SR, Mandal S, Sen A, Reber AC, Pedicini AF, Khanna SN, J. Am. Chem. Soc, 135 (2012) 26–29. [PubMed: 23237531]
- [110]. Yan J, Su H, Yang H, Malola S, Lin S, Häkkinen H, Zheng N, J. Am. Chem. Soc, 137 (2015) 11880–11883. [PubMed: 26351859]
- [111]. Biltek SR, Sen A, Pedicini AF, Reber AC, Khanna SN, The Journal of Physical Chemistry A, 118 (2014) 8314–8319. [PubMed: 24749736]
- [112]. Yuan X, Dou X, Zheng K, Xie J, Particle & Particle Systems Characterization, 32 (2015) 613–629.
- [113]. Zhang H, Watanabe T, Okumura M, Haruta M, Toshima N, Nature materials, 11 (2012) 49.
- [114]. Udayabhaskararao T, Sun Y, Goswami N, Pal SK, Balasubramanian K, Pradeep T, Angew. Chem. Int. Ed, 51 (2012) 2155–2159.
- [115]. Wang C, Xu L, Xu X, Cheng H, Sun H, Lin Q, Zhang C, J. Colloid Interface Sci, 416 (2014) 274–279. [PubMed: 24370431]
- [116]. Zhou T.-y., Lin L.-p., Rong M.-c., Jiang Y.-q., Chen X, Anal. Chem, 85 (2013) 9839–9844. [PubMed: 24016136]
- [117]. Wu Z, Angew. Chem. Int. Ed, 51 (2012) 2934–2938.
- [118]. Liu G, Feng D-Q, Zheng W, Chen T, Li D, Chem. Commun, 49 (2013) 7941–7943.
- [119]. Liao L, Zhou S, Dai Y, Liu L, Yao C, Fu C, Yang J, Wu Z, J. Am. Chem. Soc, 137 (2015) 9511–9514. [PubMed: 26196263]
- [120]. Liu X, Wang D, Li Y, Nano Today, 7 (2012) 448–466.
- [121]. Zhou C, Hao G, Thomas P, Liu J, Yu M, Sun S, Öz OK, Sun X, Zheng J, Angew. Chem. Int. Ed, 51 (2012) 10118–10122.
- [122]. Anderson CJ, Ferdani R, Cancer Biother. Radiopharm, 24 (2009) 379–393. [PubMed: 19694573]
- [123]. Zhao Y, Detering L, Sultan D, Cooper ML, You M, Cho S, Meier SL, Luehmann H, Sun G, Rettig M, ACS nano, 10 (2016) 5959. [PubMed: 27159079]
- [124]. Hu H, Huang P, Weiss OJ, Yan X, Yue X, Zhang MG, Tang Y, Nie L, Ma Y, Niu G, Biomaterials, 35 (2014) 9868–9876. [PubMed: 25224367]
- [125]. Ma X, Cheng K, Cutler C, Bu L, Sun Y, Kang F, Yang W, Wang J, Cheng Z, J. Nucl. Med, 56 (2015) 61–61.
- [126]. Le Guével X, Trouillet V, Spies C, Li K, Laaksonen T, Auerbach D, Jung G, Schneider M, Nanoscale, 4 (2012) 7624–7631. [PubMed: 23142868]
- [127]. Wang S, Meng X, Das A, Li T, Song Y, Cao T, Zhu X, Zhu M, Jin R, Angew. Chem. Int. Ed, 53 (2014) 2376–2380.
- [128]. Soldan G, Aljuhani MA, Bootharaju MS, AbdulHalim LG, Parida MR, Emwas AH, Mohammed OF, Bakr OM, Angew. Chem. Int. Ed, 55 (2016) 5749–5753.
- [129]. Zhang J, Yuan Y, Wang Y, Sun F, Liang G, Jiang Z, Yu S-H, Nano Research, 8 (2015) 2329–2339.
- [130]. Oh E, Delehanty JB, Field LD, Mäkinen AJ, Goswami R, Huston AL, Medintz IL, Chem. Mater, 28 (2016) 8676–8688.
- [131]. Zhou Q, Lin Y, Xu M, Gao Z, Yang H, Tang D, Anal. Chem, 88 (2016) 8886–8892. [PubMed: 27476555]
- [132]. Guan G, Cai Y, Liu S, Yu H, Bai S, Cheng Y, Tang T, Bharathi M, Zhang YW, Han MY, Chemistry-A European Journal, 22 (2016) 1675–1681.
- [133]. Zhai Q, Xing H, Zhang X, Li J, Wang E, Anal. Chem, 89 (2017) 7788–7794. [PubMed: 28677968]
- [134]. Huang H, Li H, Feng J-J, Wang A-J, Sensors Actuators B: Chem, 223 (2016) 550–556.
- [135]. Ristig S, Kozlova D, Meyer-Zaika W, Epple M, Journal of Materials Chemistry B, 2 (2014) 7887–7895.

- [136]. Ge W, Zhang Y, Ye J, Chen D, Rehman FU, Li Q, Chen Y, Jiang H, Wang X, JOURNAL OF NANOBIO TECHNOLOGY, 13 (2015).
- [137]. Jin R, Zeng C, Zhou M, Chen Y, Chem. Rev, 116 (2016) 10346–10413. [PubMed: 27585252]
- [138]. Wu Z, Gayathri C, Gil RR, Jin R, J. Am. Chem. Soc, 131 (2009) 6535–6542. [PubMed: 19379012]
- [139]. Wu Z, Jin R, Acs Nano, 3 (2009) 2036–2042. [PubMed: 19548695]
- [140]. Marbella LE, Millstone JE, Chem. Mater, 27 (2015) 2721–2739.
- [141]. Negishi Y, Kurashige W, Niihori Y, Iwasa T, Nobusada K, PCCP, 12 (2010) 6219–6225. [PubMed: 20393641]
- [142]. MacDonald MA, Zhang P, Qian H, Jin R, The Journal of Physical Chemistry Letters, 1 (2010) 1821–1825.
- [143]. Simms GA, Padmos JD, Zhang P, The Journal of chemical physics, 131 (2009) 214703. [PubMed: 19968356]
- [144]. MacDonald MA, Chevrier DM, Zhang P, Qian H, Jin R, The Journal of Physical Chemistry C, 115 (2011) 15282–15287.
- [145]. Zhang P, The Journal of Physical Chemistry C, 118 (2014) 25291–25299.
- [146]. Chevrier DM, Yang R, Chatt A, Zhang P, Nanotechnology Reviews, 4 (2015) 193–206.
- [147]. Petty JT, Sergev OO, Ganguly M, Rankine IJ, Chevrier DM, Zhang P, J. Am. Chem. Soc, 138 (2016) 3469–3477. [PubMed: 26924556]
- [148]. Petty JT, Ganguly M, Rankine IJ, Chevrier DM, Zhang P, The Journal of Physical Chemistry C, 121 (2017) 14936–14945.
- [149]. Padmos JD, Zhang P, The Journal of Physical Chemistry C, 116 (2012) 23094–23101.
- [150]. Padmos JD, Boudreau RT, Weaver DF, Zhang P, The Journal of Physical Chemistry C, 119 (2015) 24627–24635.
- [151]. Duchesne PN, Zhang P, Nanoscale, 4 (2012) 4199–4205. [PubMed: 22573020]
- [152]. Duchesne PN, Zhang P, The Journal of Physical Chemistry C, 118 (2014) 21714–21721.
- [153]. Chevrier DM, Zeng C, Jin R, Chatt A, Zhang P, The Journal of Physical Chemistry C, 119 (2014) 1217–1223.
- [154]. Yang R, Chevrier DM, Zeng C, Jin R, Zhang P, Can. J. Chem, (2017) 1–5.
- [155]. Liu Y, Meyer-Zaika W, Franzka S, Schmid G, Tsoli M, Kuhn H, Angew. Chem. Int. Ed, 42 (2003) 2853–2857.
- [156]. Leifert A, Pan Y, Kinkeldy A, Schiefer F, Setzler J, Scheel O, Lichtenbeld H, Schmid G, Wenzel W, Jahn-Dechent W, Proceedings of the National Academy of Sciences, 110 (2013) 8004–8009.
- [157]. Tsoli M, Kuhn H, Brandau W, Esche H, Schmid G, Small, 1 (2005) 841–844. [PubMed: 17193536]
- [158]. Jian N, Stapelfeldt C, Hu K-J, Fröba M, Palmer RE, Nanoscale, 7 (2015) 885–888. [PubMed: 25463773]
- [159]. Wang Z, Palmer R, Nano Lett, 12 (2012) 5510–5514. [PubMed: 23057610]
- [160]. Liu J, Duchesne PN, Yu M, Jiang X, Ning X, Vinluan RD, Zhang P, Zheng J, Angew. Chem, 128 (2016) 9040–9044.
- [161]. Zhu M, Aikens CM, Hollander FJ, Schatz GC, Jin R, J. Am. Chem. Soc, 130 (2008) 5883–5885. [PubMed: 18407639]
- [162]. Jin S, Wang S, Song Y, Zhou M, Zhong J, Zhang J, Xia A, Pei Y, Chen M, Li P, J. Am. Chem. Soc, 136 (2014) 15559–15565. [PubMed: 25343538]
- [163]. Chen S, Wang S, Zhong J, Song Y, Zhang J, Sheng H, Pei Y, Zhu M, Angew. Chem. Int. Ed, 54 (2015) 3145–3149.
- [164]. Weissker H-C, Escobar HB, Thanthirige V, Kwak K, Lee D, Ramakrishna G, Whetten R, López-Lozano X, Nature communications, 5 (2014) 3785.
- [165]. Devadas MS, Bairu S, Qian H, Sinn E, Jin R, Ramakrishna G, The Journal of Physical Chemistry Letters, 2 (2011) 2752–2758.
- [166]. Cirri A, Silakov A, Lear BJ, Angew. Chem. Int. Ed, 54 (2015) 11750–11753.

- [167]. Cirri A, Silakov A, Jensen L, Lear BJ, PCCP, 18 (2016) 25443–25451. [PubMed: 27711383]
- [168]. Cirri A, Silakov A, Jensen L, Lear BJ, J. Am. Chem. Soc, 138 (2016) 15987–15993. [PubMed: 27960314]
- [169]. Zheng J, Nicovich PR, Dickson RM, Annu. Rev. Phys. Chem, 58 (2007) 409–431. [PubMed: 17105412]
- [170]. Duan H, Nie S, J. Am. Chem. Soc, 129 (2007) 2412–2413. [PubMed: 17295485]
- [171]. Sharma J, Yeh H-C, Yoo H, Werner JH, Martinez JS, Chem. Commun, 46 (2010) 3280–3282.
- [172]. Negishi Y, Nobusada K, Tsukuda T, J. Am. Chem. Soc, 127 (2005) 5261–5270. [PubMed: 15810862]
- [173]. Tu X, Chen W, Guo X, Nanotechnology, 22 (2011) 095701. [PubMed: 21258146]
- [174]. Wang G, Huang T, Murray RW, Menard L, Nuzzo RG, J. Am. Chem. Soc, 127 (2005) 812–813. [PubMed: 15656600]
- [175]. Devadas MS, Kim J, Sinn E, Lee D, Goodson T III, Ramakrishna G, The Journal of Physical Chemistry C, 114 (2010) 22417–22423.
- [176]. Zhou C, Sun C, Yu M, Qin Y, Wang J, Kim M, Zheng J, The journal of physical chemistry. C, Nanomaterials and interfaces, 114 (2010) 7727.
- [177]. Zheng J, Zhou C, Yu M, Liu J, Nanoscale, 4 (2012) 4073–4083. [PubMed: 22706895]
- [178]. Weerawardene KDM, Guidez EB, Aikens CM, The Journal of Physical Chemistry C, 121 (2017) 15416–15423.
- [179]. Weerawardene KDM, Aikens CM, J. Am. Chem. Soc, 138 (2016) 11202–11210. [PubMed: 27524386]
- [180]. Pyo K, Thanthirige VD, Kwak K, Pandurangan P, Ramakrishna G, Lee D, J. Am. Chem. Soc, 137 (2015) 8244–8250. [PubMed: 26061198]
- [181]. Deng H-H, Shi X-Q, Wang F-F, Peng H-P, Liu A-L, Xia X-H, Chen W, Chem. Mater, 29 (2017) 1362–1369.
- [182]. Wu Z, Jin R, Nano Lett, 10 (2010) 2568–2573. [PubMed: 20550101]
- [183]. Pyo K, Thanthirige VD, Yoon SY, Ramakrishna G, Lee D, Nanoscale, 8 (2016) 20008–20016. [PubMed: 27782268]
- [184]. Chen Y, Montana DM, Wei H, Cordero JM, Schneider M, Le Guével X, Chen O, Bruns OT, Bawendi MG, Nano Lett, (2017).
- [185]. Zhu M, Qian H, Meng X, Jin S, Wu Z, Jin R, Nano Lett, 11 (2011) 3963–3969. [PubMed: 21834520]
- [186]. Farrag M, Tschurl M, Heiz U, Chem. Mater, 25 (2013) 862–870.
- [187]. Zeng C, Li T, Das A, Rosi NL, Jin R, J. Am. Chem. Soc, 135 (2013) 10011–10013. [PubMed: 23815445]
- [188]. Lopez-Acevedo O, Tsunoyama H, Tsukuda T, Hakkinen H, Aikens CM, J. Am. Chem. Soc, 132 (2010) 8210–8218. [PubMed: 20499877]
- [189]. Wan XK, Yuan SF, Lin ZW, Wang QM, Angew. Chem, 126 (2014) 2967–2970.
- [190]. Yang H, Yan J, Wang Y, Deng G, Su H, Zhao X, Xu C, Teo BK, Zheng N, J. Am. Chem. Soc
- [191]. Kumar J, Kawai T, Nakashima T, Chem. Commun, 53 (2017) 1269–1272.
- [192]. Yao H, Kobayashi R, J. Colloid Interface Sci, 419 (2014) 1–8. [PubMed: 24491322]
- [193]. Barrabés N, Zhang B, Buergi T, J. Am. Chem. Soc, 136 (2014) 14361–14364. [PubMed: 25251045]
- [194]. Wu Z, Chemistry-A European Journal, (2017).
- [195]. Kobayashi R, Nonoguchi Y, Sasaki A, Yao H, The Journal of Physical Chemistry C, 118 (2014) 15506–15515.
- [196]. Wang S, Jin S, Yang S, Chen S, Song Y, Zhang J, Zhu M, Science advances, 1 (2015) e1500441. [PubMed: 26601236]
- [197]. Wei J, Guo Y, Li J, Yuan M, Long T, Liu Z, Anal. Chem, 89 (2017) 9781–9787. [PubMed: 28832124]
- [198]. Ma W, Xu L, de Moura AF, Wu X, Kuang H, Xu C, Kotov NA, Chem. Rev, 117 (2017) 8041–8093. [PubMed: 28426196]

- [199]. Govan J, Gun'ko YK, Recent progress in chiral inorganic nanostructures, *Nanoscience: Volume 3*, The Royal Society of Chemistry 2016, pp. 1–30.
- [200]. He F, Yang G, Yang P, Yu Y, Lv R, Li C, Dai Y, Gai S, Lin J, *Adv. Funct. Mater*, 25 (2015) 3966–3976.
- [201]. Yang D, Yang G, Gai S, He F, An G, Dai Y, Lv R, Yang P, *Nanoscale*, 7 (2015) 19568–19578. [PubMed: 26540558]
- [202]. Yu Y, Geng J, Ong EYX, Chellappan V, Tan YN, *Advanced healthcare materials*, 5 (2016) 2528–2535. [PubMed: 27411540]
- [203]. Ho-Wu R, Yau SH, Goodson T, *The Journal of Physical Chemistry B*, (2017).
- [204]. Miyata S, Miyaji H, Kawasaki H, Nishida E, Shitomi K, Akasaka T, Tanaka S, Iizuka T, Sugaya T, *Biol*, 2 (2017) 1–4.
- [205]. Chen T, Hu Y, Cen Y, Chu X, Lu Y, *J. Am. Chem. Soc*, 135 (2013) 11595–11602. [PubMed: 23859158]
- [206]. Hu L, Deng L, Alsaiari S, Zhang D, Khashab NM, *Anal. Chem*, 86 (2014) 4989–4994. [PubMed: 24785707]
- [207]. Berezin MY, Achilefu S, *Chem. Rev*, 110 (2010) 2641. [PubMed: 20356094]
- [208]. Shang L, Azadfar N, Stockmar F, Send W, Trouillet V, Bruns M, Gerthsen D, Nienhaus GU, *Small*, 7 (2011) 2614–2620. [PubMed: 21809441]
- [209]. Shang L, Stockmar F, Azadfar N, Nienhaus GU, *Angew. Chem. Int. Ed*, 52 (2013) 11154–11157.
- [210]. Zhang KY, Yu Q, Wei H, Liu S, Zhao Q, Huang W, *Chem. Rev*, 118 (2018) 1770–1839. [PubMed: 29393632]
- [211]. Raut S, Fudala R, Rich R, Kokate R, Chib R, Gryczynski Z, Gryczynski I, *Nanoscale*, 6 (2014) 2594–2597. [PubMed: 24469148]
- [212]. Pyo K, Ly NH, Yoon SY, Shen Y, Choi SY, Lee SY, Joo S-W, Lee D, *Advanced Healthcare Materials*, 6 (2017) 1700203-n/a.
- [213]. Chen Y, Montana DM, Wei H, Cordero JM, Schneider M, Le Guével X, Chen O, Bruns OT, Bawendi MG, *Nano Lett*, 17 (2017) 6330–6334. [PubMed: 28952734]
- [214]. Basu S, Paul A, Chattopadhyay A, *Chemistry-A European Journal*, 23 (2017) 9137–9143.
- [215]. Yang S, Sun S, Zhou C, Hao G, Liu J, Ramezani S, Yu M, Sun X, Zheng J, *Bioconjugate Chem*, 26 (2015) 511–519.
- [216]. Garg S, Rong H, Miller CJ, Waite TD, *Environ. Sci. Technol*, 50 (2016) 3890–3896. [PubMed: 26986484]
- [217]. Hansen U, Thünemann AF, *Langmuir*, 31 (2015) 6842–6852. [PubMed: 26018337]
- [218]. Ahmed KBR, Nagy AM, Brown RP, Zhang Q, Malghan SG, Goering PL, *Toxicol. In Vitro*, 38 (2017) 179–192. [PubMed: 27816503]
- [219]. Liu J, Sonshine DA, Shervani S, Hurt RH, *ACS nano*, 4 (2010) 6903–6913. [PubMed: 20968290]
- [220]. Lesniak A, Fenaroli F, Monopoli MP, Åberg C, Dawson KA, Salvati A, *ACS nano*, 6 (2012) 5845–5857. [PubMed: 22721453]
- [221]. Lazarovits J, Chen YY, Sykes EA, Chan WC, *Chem. Commun*, 51 (2015) 2756–2767.
- [222]. Lee YK, Choi E-J, Webster TJ, Kim S-H, Khang D, *International journal of nanomedicine*, 10 (2015) 97. [PubMed: 25565807]
- [223]. Kopp M, Kollenda S, Epple M, *Acc. Chem. Res*, (2017).
- [224]. Perry JL, Reuter KG, Kai MP, Herlihy KP, Jones SW, Luft JC, Napier M, Bear JE, DeSimone JM, *Nano Lett*, 12 (2012) 5304–5310. [PubMed: 22920324]
- [225]. Gessner A, Lieske A, Paulke BR, Müller RH, *Eur. J. Pharm. Biopharm*, 54 (2002) 165–170. [PubMed: 12191688]
- [226]. Elci SG, Jiang Y, Yan B, Kim ST, Saha K, Moyano DF, Yesilbag Tonga G, Jackson LC, Rotello VM, Vachet RW, *ACS nano*, 10 (2016) 5536–5542. [PubMed: 27164169]
- [227]. Zhu ZJ, Posati T, Moyano DF, Tang R, Yan B, Vachet RW, Rotello VM, *Small*, 8 (2012) 2659–2663. [PubMed: 22730215]

- [228]. Porret E, Sancey L, Martín-Serrano A, Montañez MI, Seeman R, Yahia-Ammar A, Okuno H, Gomez F, Ariza A, Hildebrandt N, *Chem. Mater*, 29 (2017) 7497–7506.
- [229]. Garcia KP, Zarschler K, Barbaro L, Barreto JA, O'Malley W, Spiccia L, Stephan H, Graham B, *Small*, 10 (2014) 2516–2529. [PubMed: 24687857]
- [230]. Choi HS, Ipe BI, Misra P, Lee JH, Bawendi MG, Frangioni JV, *Nano Lett*, 9 (2009) 2354–2359. [PubMed: 19422261]
- [231]. Ning X, Peng C, Li ES, Xu J, Vinluan RD III, Yu M, Zheng J, *Apl Materials*, 5 (2017) 053406. [PubMed: 29667805]
- [232]. Zhou C, Long M, Qin Y, Sun X, Zheng J, *Angew. Chem*, 123 (2011) 3226–3230.
- [233]. Liu J, Yu M, Ning X, Zhou C, Yang S, Zheng J, *Angew. Chem. Int. Ed*, 52 (2013) 12572–12576.
- [234]. Zhou M, Li J, Liang S, Sood AK, Liang D, Li C, *ACS nano*, 9 (2015) 7085–7096. [PubMed: 26098195]
- [235]. Yang W, Liu S, Bai T, Keefe AJ, Zhang L, Ella-Menye J-R, Li Y, Jiang S, *Nano Today*, 9 (2014) 10–16.
- [236]. Longmire M, Choyke PL, Kobayashi H, *Nanomedicine*, 3 (2008) 703–717. [PubMed: 18817471]
- [237]. Zhang Y-N, Poon W, Tavares AJ, McGilvray ID, Chan WC, *J. Controlled Release*, 240 (2016) 332–348.
- [238]. Yu M, Zheng J, *ACS nano*, 9 (2015) 6655–6674. [PubMed: 26149184]
- [239]. Rai M, Yadav A, Gade A, *Biotechnol. Adv*, 27 (2009) 76–83. [PubMed: 18854209]
- [240]. Prabhu S, Poulouse EK, *International Nano Letters*, 2 (2012) 32.
- [241]. Yuan X, Setyawati MI, Leong DT, Xie J, *Nano Research*, 7 (2014) 301–307.
- [242]. Yuan X, Setyawati MI, Tan AS, Ong CN, Leong DT, Xie J, *NPG Asia Materials*, 5 (2013) e39.
- [243]. K rösi L, Rodio M, Dömötör D, Kovács T, Papp S, Diaspro A, Intartaglia R, Beke S, *Journal of Chemistry*, 2016 (2016).
- [244]. Zheng K, Setyawati MI, Lim T-P, Leong DT, Xie J, *ACS nano*, 10 (2016) 7934–7942. [PubMed: 27494437]
- [245]. An D, Su J, Weber JK, Gao X, Zhou R, Li J, *J. Am. Chem. Soc*, 137 (2015) 8412–8418. [PubMed: 26084190]
- [246]. Wu Z, Zhang B, Yan B, *Int. J. Mol. Sci*, 10 (2009) 4198–4209. [PubMed: 20057940]
- [247]. Fischer NO, McIntosh CM, Simard JM, Rotello VM, *Proceedings of the National Academy of Sciences*, 99 (2002) 5018–5023.
- [248]. Chakraborty S, Babanova S, Rocha RC, Desireddy A, Artyushkova K, Boncella AE, Atanassov P, Martinez JS, *J. Am. Chem. Soc*, 137 (2015) 11678–11687. [PubMed: 26288369]
- [249]. Weissleder R, Nahrendorf M, Pittet MJ, *Nature materials*, 13 (2014) 125–138. [PubMed: 24452356]
- [250]. Vinluan RD III, Yu M, Gannaway M, Sullins J, Xu J, Zheng J, *Bioconjugate Chem*, 26 (2015) 2435–2441.
- [251]. Liu CL, Wu HT, Hsiao YH, Lai CW, Shih CW, Peng YK, Tang KC, Chang HW, Chien YC, Hsiao JK, *Angew. Chem. Int. Ed*, 50 (2011) 7056–7060.
- [252]. Yu M, Liu J, Ning X, Zheng J, *Angew. Chem. Int. Ed*, 54 (2015) 15434–15438.
- [253]. Yu M, Zhou J, Du B, Ning X, Authement C, Gandee L, Kapur P, Hsieh JT, Zheng J, *Angew. Chem*, 128 (2016) 2837–2841.
- [254]. Xu J, Yu M, Carter P, Hernandez E, Dang A, Kapur P, Hsieh JT, Zheng J, *Angew. Chem. Int. Ed*, (2017).
- [255]. Hainfeld J, Slatkin D, Focella T, Smilowitz H, *The British journal of radiology*, 79 (2006) 248–253. [PubMed: 16498039]
- [256]. Chen F, Goel S, Hernandez R, Graves SA, Shi S, Nickles RJ, Cai W, *small*, 12 (2016) 2775–2782. [PubMed: 27062146]
- [257]. Alric C, Miladi I, Kryza D, Taleb J, Lux F, Bazzi R, Billotey C, Janier M, Perriat P, Roux S, *Nanoscale*, 5 (2013) 5930–5939. [PubMed: 23702968]



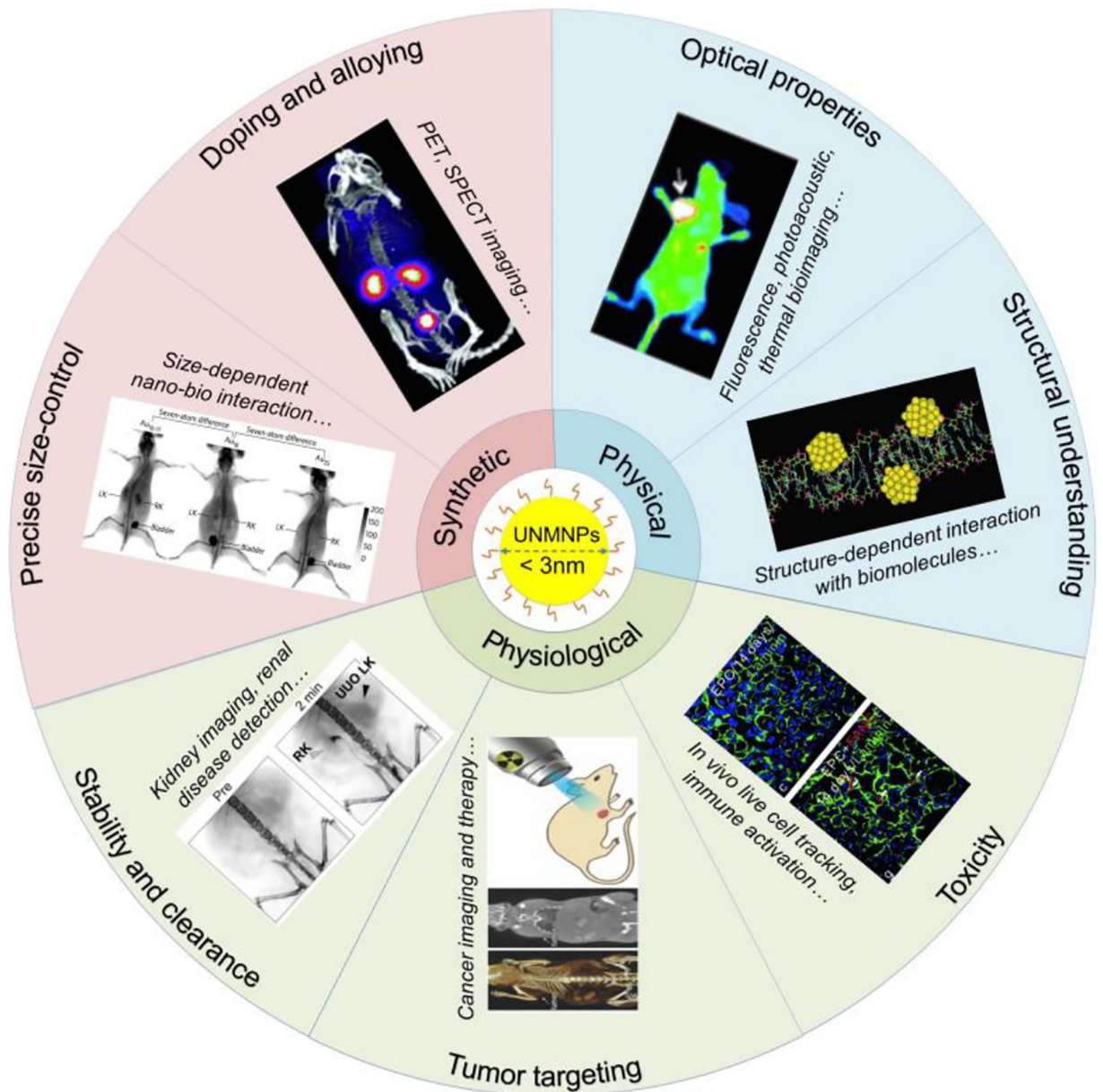
- [258]. Alric C, Taleb J, Duc GL, Mandon C, Billotey C, Meur-Herland AL, Brochard T, Vocanson F, Janier M, Perriat P, *J. Am. Chem. Soc.*, 130 (2008) 5908–5915. [PubMed: 18407638]
- [259]. Liang G, Ye D, Zhang X, Dong F, Chen H, Zhang S, Li J, Shen X, Kong J, *Journal of Materials Chemistry B*, 1 (2013) 3545–3552.
- [260]. Fukumura D, Jain RK, *APMIS*, 116 (2008) 695–715 [PubMed: 18834413]
- [261]. Maeda H, *Adv. Enzyme Regul.*, 41 (2001) 189–207. [PubMed: 11384745]
- [262]. Liu J, Yu M, Zhou C, Yang S, Ning X, Zheng J, *J. Am. Chem. Soc.*, 135 (2013) 4978–4981. [PubMed: 23506476]
- [263]. Toy R, Peiris PM, Ghaghada KB, Karathanasis E, *Nanomedicine*, 9 (2014) 121–134. [PubMed: 24354814]
- [264]. Müller K, Fedosov DA, Gompper G, *Scientific reports*, 4 (2014) 4871. [PubMed: 24786000]
- [265]. Toy R, Hayden E, Shoup C, Baskaran H, Karathanasis E, *Nanotechnology*, 22 (2011) 115101. [PubMed: 21387846]
- [266]. Carboni E, Tschudi K, Nam J, Lu X, Ma AW, *AAPS PharmSciTech*, 15 (2014) 762–771. [PubMed: 24687242]
- [267]. Blanco E, Shen H, Ferrari M, *Nat. Biotechnol.*, 33 (2015) 941–951. [PubMed: 26348965]
- [268]. Zarschler K, Rocks L, Licciardello N, Boselli L, Polo E, Garcia KP, De Cola L, Stephan H, Dawson KA, *Nanomedicine: Nanotechnology, Biology and Medicine*, 12 (2016) 1663–1701.
- [269]. Bazak R, Hourri M, El Achy S, Kamel S, Refaat T, *Cancer Res J. Clin. Oncol.*, 141 (2015) 769–784.
- [270]. Kue CS, Kamkaew A, Burgess K, Kiew LV, Chung LY, Lee HB, *Med. Res. Rev.*, 36 (2016) 494–575. [PubMed: 26992114]
- [271]. Bertrand N, Wu J, Xu X, Kamaly N, Farokhzad OC, *Advanced drug delivery reviews*, 66 (2014) 2–25. [PubMed: 24270007]
- [272]. Stefanick JF, Ashley JD, Kiziltepe T, Bilgicer B, *ACS nano*, 7 (2013) 2935–2947. [PubMed: 23421406]
- [273]. Elias DR, Poloukhine A, Popik V, Tsourkas A, *Nanomedicine: nanotechnology, biology and medicine*, 9 (2013) 194–201.
- [274]. Jain RK, Stylianopoulos T, *Nature reviews Clinical oncology*, 7 (2010) 653–664.
- [275]. Ferrari M, *Trends Biotechnol.*, 28 (2010) 181–188. [PubMed: 20079548]
- [276]. Sykes EA, Chen J, Zheng G, Chan WC, (2014).
- [277]. Huang K, Ma H, Liu J, Huo S, Kumar A, Wei T, Zhang X, Jin S, Gan Y, Wang PC, *ACS nano*, 6 (2012) 4483–4493. [PubMed: 22540892]
- [278]. Peng C, Gao X, Xu J, Du B, Ning X, Tang S, Bachoo RM, Yu M, Ge W-P, Zheng J, *Nano research*, 10 (2017) 1366–1376. [PubMed: 29034063]
- [279]. Huo S, Jin S, Ma X, Xue X, Yang K, Kumar A, Wang PC, Zhang J, Hu Z, Liang X-J, *ACS nano*, 8 (2014) 5852–5862. [PubMed: 24824865]
- [280]. Zhang P, Yang XX, Wang Y, Zhao NW, Huang CZ, *Nanoscale*, 6 (2014) 2261–2269. [PubMed: 24407194]
- [281]. Zhang C, Li C, Liu Y, Zhang J, Bao C, Liang S, Wang Q, Yang Y, Fu H, Wang K, *Adv. Funct. Mater.*, 25 (2015) 1314–1325.
- [282]. Chen H, Li S, Li B, Ren X, Li S, Mahounga DM, Cui S, Gu Y, Achilefu S, *Nanoscale*, 4 (2012) 6050–6064. [PubMed: 22930451]
- [283]. Huo S, Chen S, Gong N, Liu J, Li X, Zhao Y, Liang X-J, *Bioconjugate Chem*, 28 (2016) 239–243.
- [284]. Jiang X, Du B, Yu M, Jia X, Zheng J, *Journal of Innovative Optical Health Sciences*, 9 (2016) 1642003.
- [285]. Fernández TD, Pearson JR, Leal MP, Torres MJ, Blanca M, Mayorga C, Le Guével X, *Biomaterials*, 43 (2015) 1–12. [PubMed: 25591956]
- [286]. Verma A, Stellacci F, *Small*, 6 (2010) 12–21. [PubMed: 19844908]
- [287]. Yu M, Zhou C, Liu J, Hankins JD, Zheng J, *J. Am. Chem. Soc.*, 133 (2011) 11014–11017. [PubMed: 21714577]

- [288]. Yu M, Zhou C, Liu L, Zhang S, Sun S, Hankins JD, Sun X, Zheng J, *Angew. Chem*, 129 (2017) 4378–4383.
- [289]. Miladi I, Alric C, Dufort S, Mowat P, Dutour A, Mandon C, Laurent G, Bräuer-Krisch E, Herath N, Coll JL, *Small*, 10 (2014) 1116–1124. [PubMed: 24659273]
- [290]. Hu D-H, Sheng Z-H, Zhang P-F, Yang D-Z, Liu S-H, Gong P, Gao D-Y, Fang S-T, Ma Y-F, Cai L-T, *Nanoscale*, 5 (2013) 1624–1628. [PubMed: 23334397]
- [291]. Zhang X-D, Luo Z, Chen J, Song S, Yuan X, Shen X, Wang H, Sun Y, Gao K, Zhang L, *Scientific reports*, 5 (2015) 8669. [PubMed: 25727895]
- [292]. Zhang XD, Chen J, Luo Z, Wu D, Shen X, Song SS, Sun YM, Liu PX, Zhao J, Huo S, *Advanced healthcare materials*, 3 (2014) 133–141. [PubMed: 23873780]
- [293]. Liang G, Jin X, Zhang S, Xing D, *Biomaterials*, 144 (2017) 95–104. [PubMed: 28834765]
- [294]. Porcel E, Liehn S, Remita H, Usami N, Kobayashi K, Furusawa Y, Le Sech C, Lacombe S, *Nanotechnology*, 21 (2010) 085103.
- [295]. Pedone D, Moglianetti M, De Luca E, Bardi G, Pompa PP, *Chem. Soc. Rev*, 46 (2017) 4951–4975. [PubMed: 28696452]
- [296]. Zhou F, Feng B, Yu H, Wang D, Wang T, Liu J, Meng Q, Wang S, Zhang P, Zhang Z, *Theranostics*, 6 (2016) 679. [PubMed: 27022415]
- [297]. Nair LV, Nazeer SS, Jayasree RS, Ajayaghosh A, *ACS nano*, 9 (2015) 5825–5832. [PubMed: 25970038]
- [298]. Talcott B, Moore MS, *Trends Cell Biol*, 9 (1999) 312–318. [PubMed: 10407410]
- [299]. Zhang X, Chibli H, Mielke R, Nadeau J, *Bioconjugate Chem*, 22 (2010) 235–243.
- [300]. Zhang X, Shastry S, Bradforth SE, Nadeau JL, *Nanoscale*, 7 (2015) 240–251. [PubMed: 25407725]
- [301]. Zhang X, Teodoro JG, Nadeau JL, *Nanomedicine: Nanotechnology, Biology and Medicine*, 11 (2015) 1365–1375.
- [302]. Wang Y, Chen J, Irudayaraj J, *ACS nano*, 5 (2011) 9718–9725. [PubMed: 22053819]
- [303]. Vankayala R, Kuo CL, Nuthalapati K, Chiang CS, Hwang KC, *Adv. Funct. Mater*, 25 (2015) 5934–5945.
- [304]. Fischer HC, Chan WC, *Curr. Opin. Biotechnol*, 18 (2007) 565–571. [PubMed: 18160274]
- [305]. Yang L, Kuang H, Zhang W, Aguilar ZP, Wei H, Xu H, *Scientific Reports*, 7 (2017).
- [306]. Bar-Ilan O, Albrecht RM, Fako VE, Furgeson DY, *Small*, 5 (2009) 1897–1910. [PubMed: 19437466]
- [307]. Tiedemann D, Taylor U, Rehbock C, Jakobi J, Klein S, Kues WA, Barcikowski S, Rath D, *Analyst*, 139 (2014) 931–942. [PubMed: 24171189]
- [308]. Haase A, Tentschert J, Jungnickel H, Graf P, Manton A, Draude F, Plendl J, Goetz M, Galla S, Maši A, *Journal of Physics: Conference Series*, IOP Publishing 2011, pp. 012030.
- [309]. Asharani P, Lianwu Y, Gong Z, Valiyaveetil S, *Nanotoxicology*, 5 (2011) 43–54. [PubMed: 21417687]
- [310]. Das B, Tripathy S, Adhikary J, Chattopadhyay S, Mandal D, Dash SK, Das S, Dey A, Dey SK, Das D, *JBIC Journal of Biological Inorganic Chemistry*, 22 (2017) 893–918. [PubMed: 28643149]
- [311]. El Badawy AM, Silva RG, Morris B, Scheckel KG, Suidan MT, Tolaymat TM, *Environ. Sci. Technol*, 45 (2010) 283–287. [PubMed: 21133412]
- [312]. Fröhlich E, *International journal of nanomedicine*, 7 (2012) 5577. [PubMed: 23144561]
- [313]. Arvizo RR, Miranda OR, Thompson MA, Pabelick CM, Bhattacharya R, Robertson JD, Rotello VM, Prakash Y, Mukherjee P, *Nano Lett*, 10 (2010) 2543–2548. [PubMed: 20533851]
- [314]. Goodman CM, McCusker CD, Yilmaz T, Rotello VM, *Bioconjugate Chem*, 15 (2004) 897–900.
- [315]. Lin J, Zhang H, Chen Z, Zheng Y, *ACS nano*, 4 (2010) 5421–5429. [PubMed: 20799717]
- [316]. Lesniak A, Salvati A, Santos-Martinez MJ, Radomski MW, Dawson KA, Åberg C, *J. Am. Chem. Soc*, 135 (2013) 1438–1444. [PubMed: 23301582]
- [317]. Shang L, Dörlich RM, Trouillet V, Bruns M, Nienhaus GU, *Nano Research*, 5 (2012) 531–542.

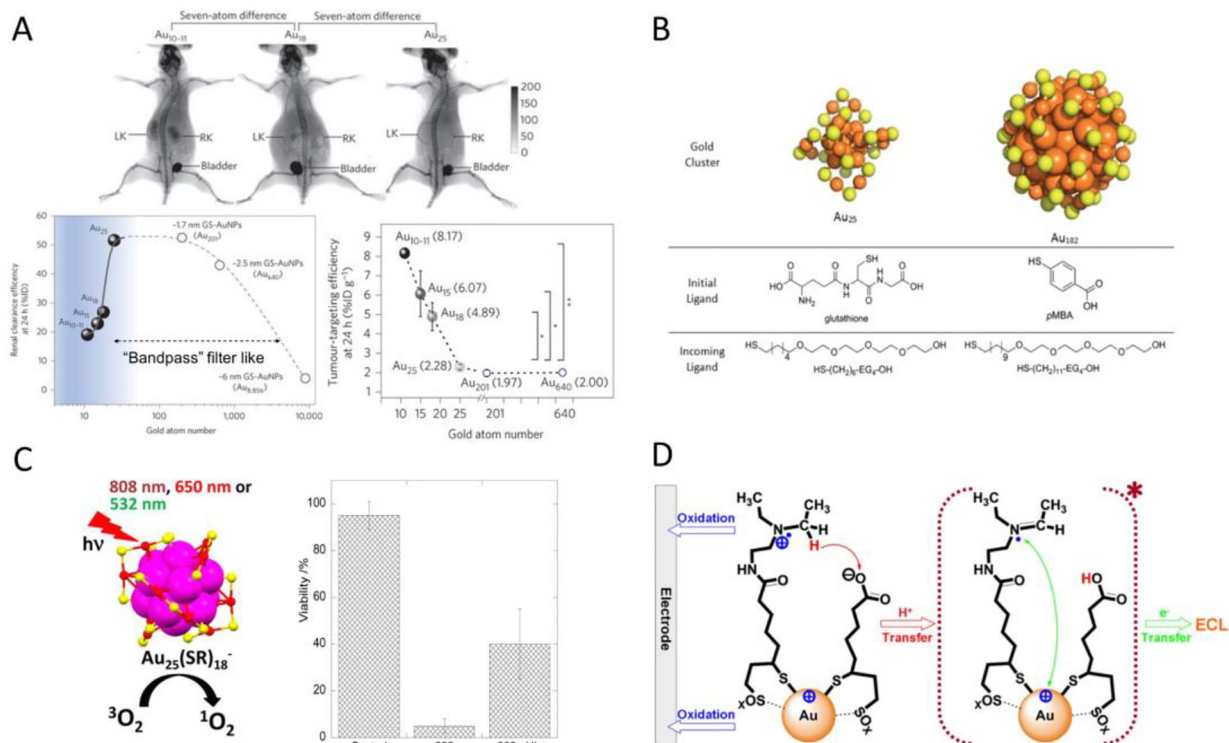
- [318]. Cho W-S, Cho M, Jeong J, Choi M, Cho H-Y, Han BS, Kim SH, Kim HO, Lim YT, Chung BH, Toxicol. Appl. Pharmacol, 236 (2009) 16–24. [PubMed: 19162059]
- [319]. Sabella S, Carney RP, Brunetti V, Malvindi MA, Al-Juffali N, Vecchio G, Janes SM, Bakr OM, Cingolani R, Stellacci F, Nanoscale, 6 (2014) 7052–7061. [PubMed: 24842463]
- [320]. Manke A, Wang L, Rojanasakul Y, BioMed research international, 2013 (2013).
- [321]. Zheng J, Xu J, Yu M, Peng C, Carter P, Tian J, Ning X, Zhou Q, Tu Q, Zhang G, Angew. Chem. Int. Ed, (2017).
- [322]. Wang H-H, Lin C-AJ, Lee C-H, Lin Y-C, Tseng Y-M, Hsieh C-L, Chen C-H, Tsai C-H, Hsieh C-T, Shen J-L, ACS nano, 5 (2011) 4337–4344. [PubMed: 21608984]
- [323]. Yang L, Shang L, Nienhaus GU, Nanoscale, 5 (2013) 1537–1543. [PubMed: 23322237]
- [324]. Yangzhouyun X, Yong L, Junchuan Y, Yuan L, Fupin H, Kui Z, Xingyu J, Angew. Chem. Int. Ed, 57 (2018) 3958–3962.
- [325]. Tao Y, Ju E, Li Z, Ren J, Qu X, Adv. Funct. Mater, 24 (2014) 1004–1010.
- [326]. Chen H, Dorrigan A, Saad S, Hare DJ, Cortie MB, Valenzuela SM, PLoS One, 8 (2013) e58208. [PubMed: 23469154]
- [327]. Wong KK, Liu X, MedChemComm, 1 (2010) 125–131.

**Highlight**

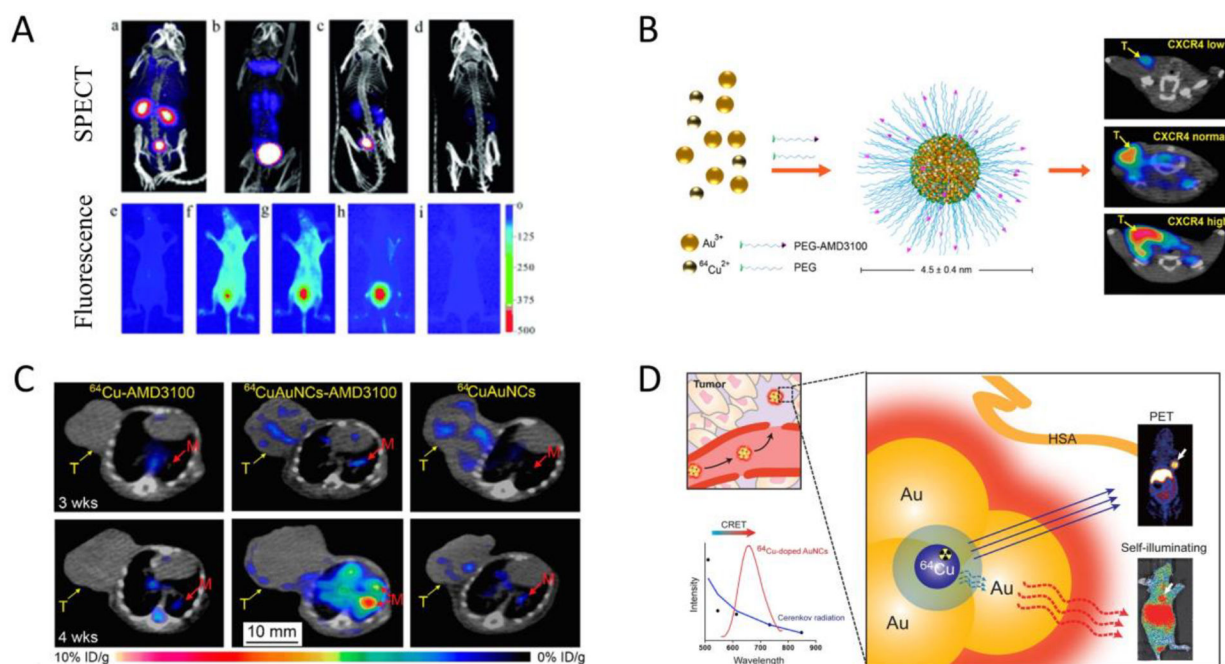
- With decades' efforts, significant breakthroughs in the synthesis, characterization and functionalization of ultrasmall noble metal
- nanoparticles lead to many unique applications in the healthcare, which cannot be readily achieved with other nanomaterials In
- this review, we summarized these advances...



**Fig.1.** Illustration of the diverse biomedical applications of UNMNPs enabled by the breakthroughs of their synthesis as well as physical and physiological properties. Representative images are adapted from Ref. [63], [67], [121], [155], [233], [254] and [322] with permissions from respective publishers.

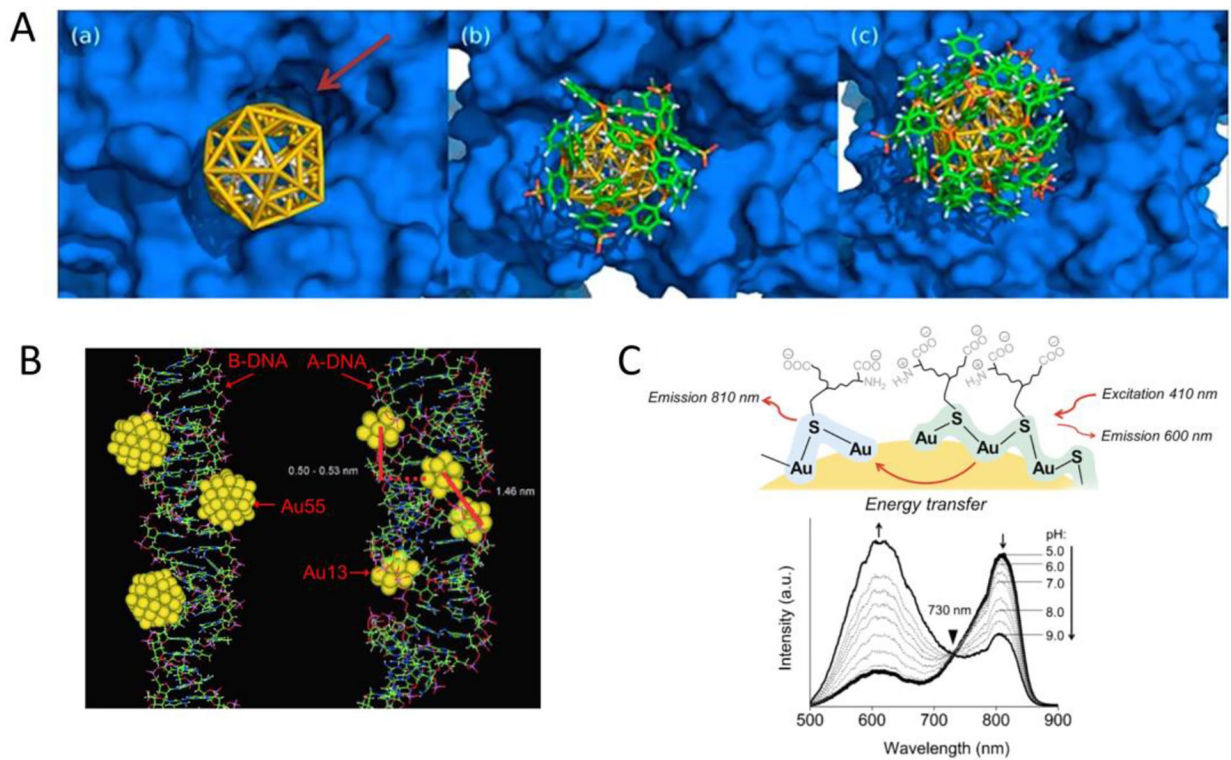
**Fig.2.**

(A) Whole-body X-ray images of mice after i.v. injection of  $Au_{10-11}$ ,  $Au_{18}$  and  $Au_{25}$  at 40min post injection. The smallest  $Au_{10-11}$  is retained in kidney much longer than  $Au_{18}$ , which is in turn longer than  $Au_{25}$ , although all three AuNCs are cleared through kidneys into the bladder (top). Renal clearance efficiency of glutathione protected  $Au_{10-11}$ ,  $Au_{15}$ ,  $Au_{18}$ ,  $Au_{25}$ , 1.7nm (~ $Au_{201}$ ), 2.5nm (~ $Au_{640}$ ) and 6nm (~ $Au_{8856}$ ) AuNPs at 24h post i.v. injection, embodying the kidney glomerulus filtration as an atomically precise ‘bandpass’ barrier (bottom left). Passive tumor targeting efficiency of glutathione protected  $Au_{10-11}$ ,  $Au_{15}$ ,  $Au_{18}$ ,  $Au_{25}$ ,  $Au_{201}$  and  $Au_{640}$  at 24h post i.v. injection (bottom right). (B) Structures of each molecular component used in the ligand replacement study. (C) Schematic illustration of efficient singlet oxygen generation by  $Au_{25}(SR)_{18}$  nanoclusters under visible/NIR (532, 650, and 808nm) light irradiation (left). *In vitro* experiments demonstrate  $Au_{25}(Capt)_{18}$  - nanoclusters can efficiently kill Hela cells photodynamically under 808nm light irradiation (right). (D) Scheme of stepwise NIR ECL generation from lipoic acid stabilized  $Au_{22}$  nanoclusters (Au-LA) conjugated with coreactants N,N-diethylethylenediamine (DEDA). (Adapted or reprinted with permissions from *Springer Nature* for (A) Ref. [63], *Royal Society of Chemistry* for (B) Ref. [64], *American Chemical Society* for (C) Ref. [66] and (D) Ref. [85].)



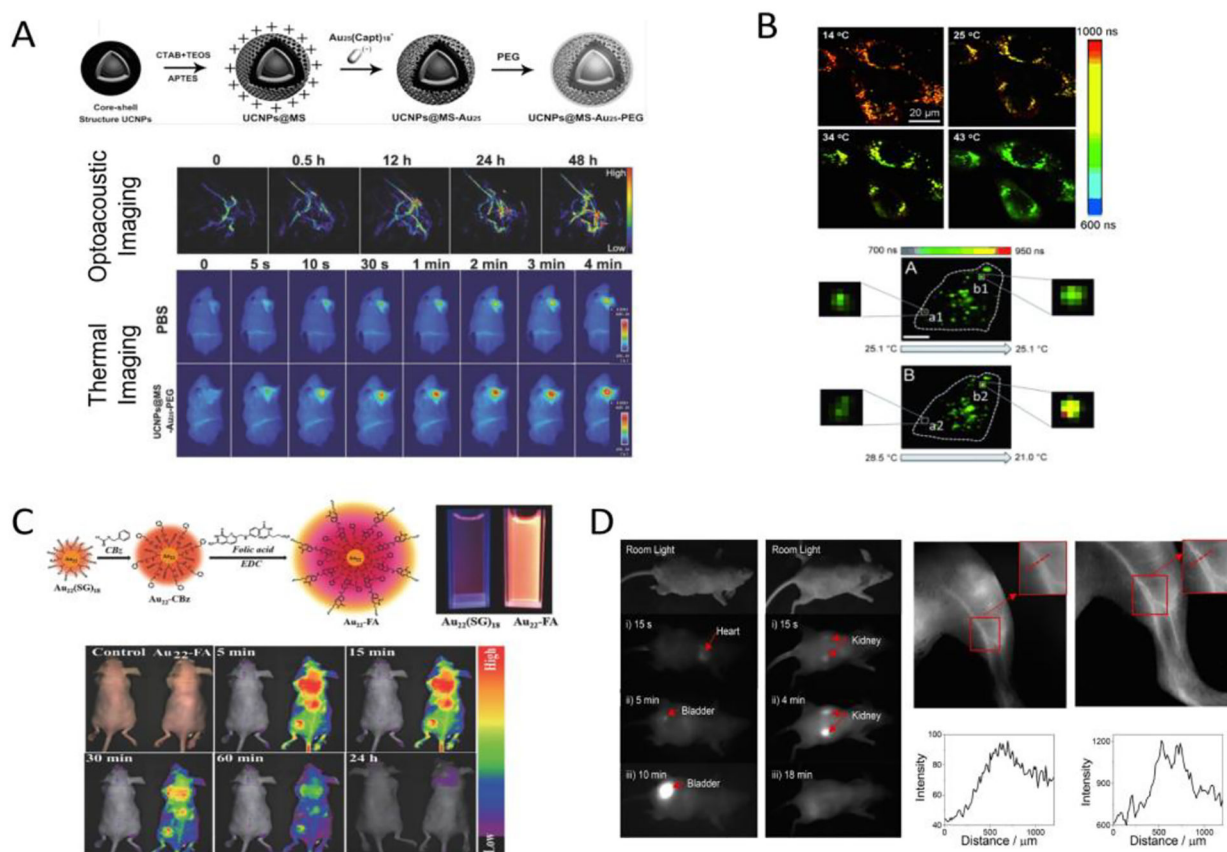
**Fig.3.**

(A) Representative SPECT (top) and NIR fluorescence (bottom) *in vivo* imaging of mice at multiple time points after IV injection of  $^{198}\text{Au}$  doped ultrasmall renal clearable GS- $^{98}\text{Au}$  AuNPs. (B) Schematic of  $^{64}\text{Cu}$  doped gold nanocluster functionalized with active targeting ligand AMD3100 ( $^{64}\text{CuAuNCs-AMD3100}$ ) for targeted PET imaging of breast cancer in mouse models expressing different levels of CXCR4 receptors. (C) Representative PET/CT transverse images of  $^{64}\text{CuAuNCs-AMD3100}$  targeting 4T1 breast cancer lung metastasis as compared to that of  $^{64}\text{Cu-AMD3100}$  and  $^{64}\text{CuAuNCs}$  alone at 3 and 4 weeks after tumor implantation. (D) Scheme of self-illuminating  $^{64}\text{Cu}$ -doped gold nanoclusters for *in vivo* dual-modality PET and CRET-based NIR fluorescence tumor imaging. (Adapted or reprinted with permissions from *John Wiley and Sons* for (A) Ref. [121], *American Chemical Society* for (B and C) Ref. [123], *Elsevier* for (D) Ref. [125].)

**Fig.4.**

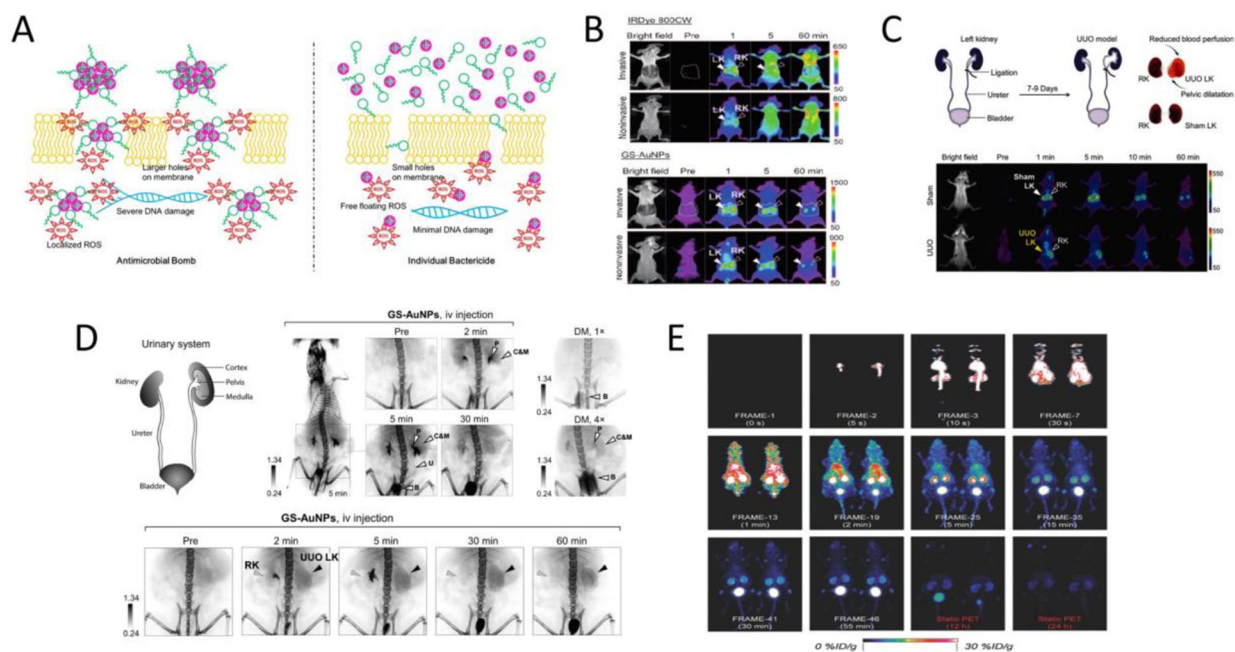
(A) Molecular simulation of 1.4nm TPPMS-coated Au<sub>55</sub> nanocluster docking to the intracellular hERG channel: bare Au<sub>55</sub> core without TPPMS ligands (left), Au<sub>55</sub> partially covered with 6 TPPMS ligands (middle), and Au<sub>55</sub> covered with 12 TPPMS ligands (right). (B) Simulation of Au<sub>55</sub> and Au<sub>13</sub> clusters interacting with the major grooves of energy-minimized B-DNA and A-DNA, respectively. (C) Schematic representation of the energy transfer from a 600nm emission center to a 810nm emission center on one ultrasmall dual-emissive GS-AuNP (top); luminescence spectra of the dual-emissive GS-AuNPs in PBS buffer at various pH values (bottom). (Adapted or reprinted with permissions from *National Academy of Sciences* for (A) Ref. [156], *John Wiley and Sons* for (B) Ref. [155] and (C) Ref. [160].)



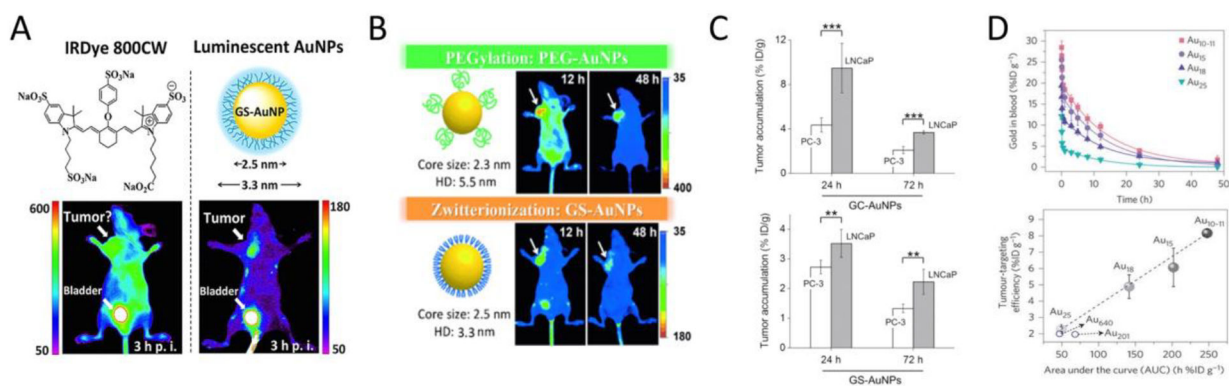


**Fig.5.**

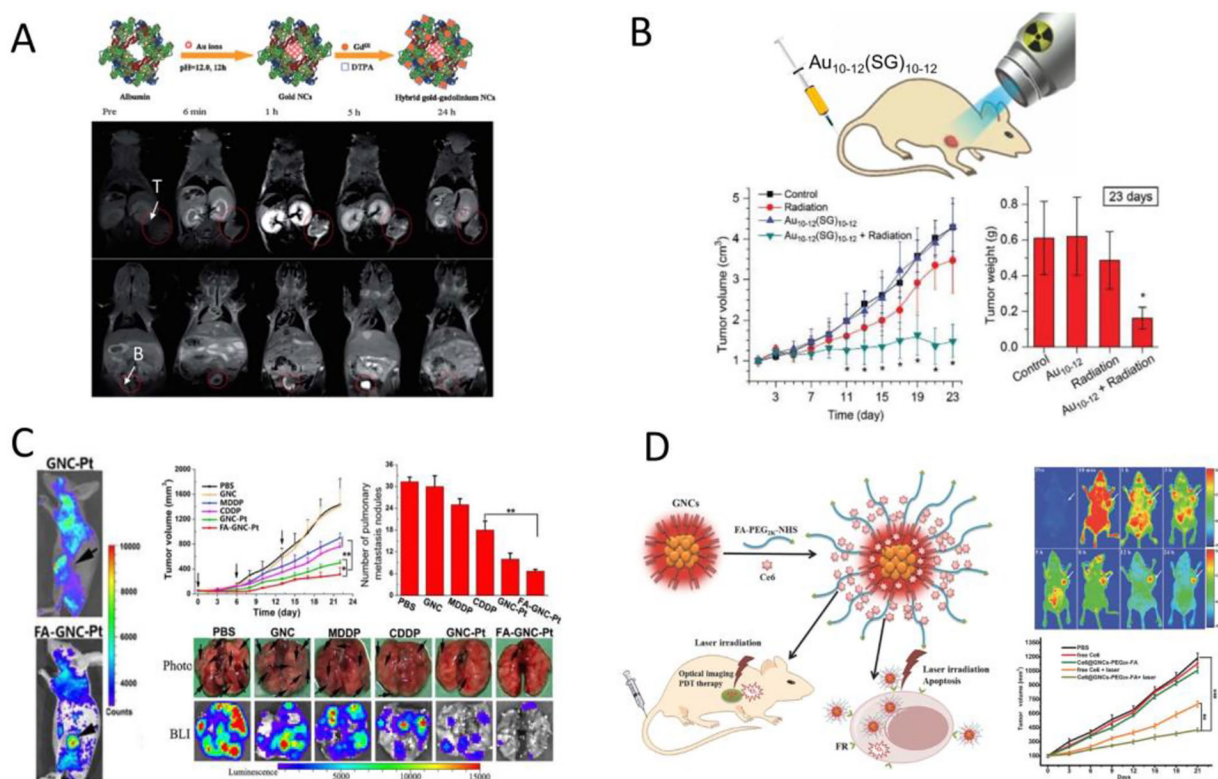
(A) Schematic illustration for the fabrication of Au<sub>25</sub> loaded mesoporous silica shell coating outside of upconversion nanoparticles (UCNPs@MS-Au<sub>25</sub>-PEG) (top); *in vivo* photoacoustic imaging of tumor tissues after IV injection of UCNPs@MS-Au<sub>25</sub>-PEG and thermal imaging of H22 tumor-bearing mice exposed to 808nm laser after IV injection of PBS or UCNPs@MS-Au<sub>25</sub>-PEG (bottom). (B) Typical fluorescence lifetime microscopy images of HeLa cells with internalized AuNCs at four different temperatures (top); temperature variations inside a single HeLa cell as revealed by the fluorescence lifetime imaging of internalized AuNCs (bottom). (C) Schematic of the synthetic route from Au<sub>22</sub>(SG)<sub>18</sub> to Au<sub>22</sub>-FA and the representative luminescence of Au<sub>22</sub>(SG)<sub>18</sub> and Au<sub>22</sub>-FA clusters with the same optical density under 365nm UV lamp irradiation (top); representative *in vivo* luminescence images of mice IV injected with saline (control) or Au<sub>22</sub>-FA (bottom). (D) Time series of the *in vivo* fluorescence images taken from the front side as well as back side of a mouse after IV injection of the long emission-wavelength AuNPs (left); fluorescence imaging of the blood vessels in the leg of a mouse injected with the AuNPs using a silicon camera with 850nm LP filter or 1250nm LP filter (right). (Adapted or reprinted with permissions from *John Wiley and Sons* for (A) Ref. [200], (B) Ref. [209] and (C) Ref. [212], *American Chemical Society* for (D) Ref. [213].)



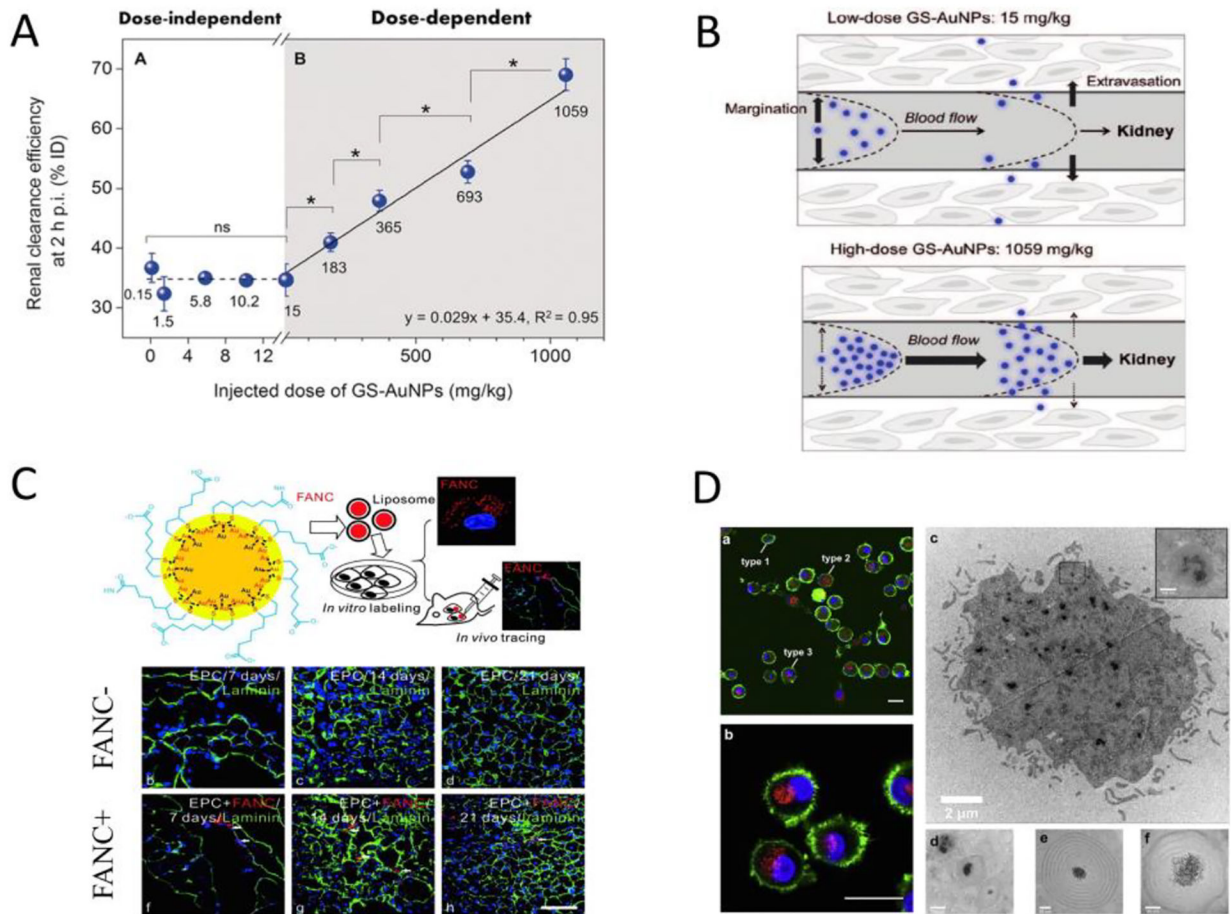
**Fig.6.** (A) Schematic representation of the different antimicrobial efficacy resulting from antimicrobial bomb (silver nanoclusters conjugated with daptomycin) (left) or individual bactericide (physical mixture) (right). (B) Whole-body invasive and noninvasive fluorescence images of mice after IV injection of IRDye 800CW (top) or NIR-emitting GS-AuNPs (bottom). (C) Illustration of the surgical operation for the establishment of unilateral ureteral obstruction (UUO) mouse model (top) and representative whole-body noninvasive fluorescence images of sham operated mice or UUO mice injected with NIR-emitting GS-AuNPs (bottom). (D) Representative X-ray images of mice after IV injection of renal clearable GS-AuNPs at various time points as compared to that of mice injected with two doses of diatrizoate meglumine (DM, clinical iodine contrast agent) at their maximum contrast enhancements (top); representative X-ray images of the urinary system in UUO mice after IV injection of the GS-AuNPs (bottom). (E) Dynamic PET imaging of the renal clearance of <sup>64</sup>Cu labeled ultrasmall AuNPs (<sup>64</sup>Cu-NOTA-Au-GSH) after IV injection in mice. (Adapted or reprinted with permissions from *American Chemical Society* for (A) Ref. [244], *John Wiley and Sons* for (B) Ref. [252], (C) Ref. [253], (D) Ref. [254] and (E) Ref. [256].)



**Fig.7.** (A) Representative *in vivo* NIR fluorescence images of MCF-7 tumor-bearing mice IV injected with either IRDye 800CW (left) or ultrasmall luminescent GS-AuNPs (right) at 3h post injection. (B) Comparison of *in vivo* NIR fluorescence imaging of ultrasmall antifouling PEG-coated AuNPs (top) and glutathione-coated AuNPs (bottom) in MCF-7 tumor bearing mice at 12h and 48h post IV injection. (C) Tumor targeting efficiency of ultrasmall acidity-targeting GC-AuNPs in PC-3 tumor model (extracellular pH=6.9) and LNCaP tumor model (extracellular pH=6.5) at two different time points post IV injection (top) as compared to that of ultrasmall GS-AuNPs without acidity-targeting ability (bottom). (D) Blood pharmacokinetics of glutathione coated Au10–11, Au15, Au18 and Au25 nanoclusters (top); the linear relationship between tumortargeting efficiencies at 24h p.i. and area under the pharmacokinetics curve (AUC) indicates that tumor targeting of these AuNCs stem from the EPR effect (bottom). (Adapted or reprinted with permissions from *American Chemical Society* for (A) Ref. [262], *John Wiley and Sons* for (B) Ref. [233] and (C) Ref. [288], *Springer Nature* for (D) Ref. [63].)

**Fig.8.**

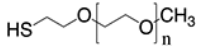
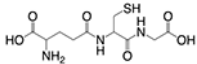
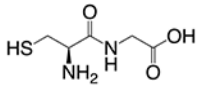
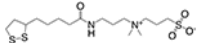
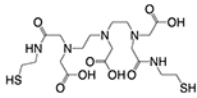
(A) Schematic of the synthetic route to the hybrid gold-gadolinium nanoclusters (top); *in vivo* MRI images of MCF-7 tumor-bearing mice (tumor and bladder were indicated) at multiple time points after IV injection of the hybrid gold-gadolinium nanoclusters (bottom). (B) Illustration of ultrasmall Au<sub>10-12</sub>(SG)<sub>10-12</sub> nanoclusters as cancer radiosensitizers (top); time-course studies of the tumor volumes and tumor weights (at 23 days post injection) for different experimental groups after radiation therapy (bottom). (C) *In vivo* fluorescence imaging of the cisplatin prodrug conjugated fluorescent gold nanocluster (GNC-Pt) and GNC-Pt linked with folic acid (FA-GNC-Pt) in 4T1 tumor-bearing mice (left); anti-cancer efficacy of FA-GNC-Pt and other control studies on the 4T1 primary tumor volume as well as the number of lung metastasis nodules examined by bright field and bioluminescence imaging (right). (D) Schematic illustration of the preparation of the folic acid-conjugated photosensitizer (Ce6)-loaded fluorescent AuNCs (Ce6@GNCs-PEG-FA) and their applications in targeted imaging and photodynamic therapy (left); *in vivo* fluorescence imaging and tumor growth trend after photodynamic therapy using Ce6@GNCs-PEG-FA (right). (Adapted or reprinted with permissions from *Royal Society of Chemistry* for (A) Ref. [290], *John Wiley and Sons* for (B) Ref. [67] and (D) Ref. [281], *Ivyspring International Publisher* for (C) Ref. [296].)



**Fig.9.** (A) Dose effect on the renal clearance of ultrasmall GS-AuNPs after IV injection in CD-1 mice. (B) Illustration of the dose-dependent transport of GS-AuNPs in blood vessels: at low dose, GS-AuNPs marginate extensively and readily enter the extravascular space (top), while in the case of high dose GS-AuNPs tend to be confined in blood vessels with reduced extravasation (bottom), resulting in more rapid transport within blood vessels and higher renal clearance. (C) Schematic of the delivery of fluorescent gold nanoclusters (FANC) into live cells as biocompatible fluorescent labels via liposome complex method (top); confocal images of stained calf muscles from hindlimb ischemic mice injected with endothelial progenitor cells labeled with or without FANC at 7, 14 and 21 days post injection (bottom). (D) Confocal laser scanning microscopy images (left) and transmission electron microscopy images (right) of fluorescent AuNCs internalized by human dendritic cells. (Adapted or reprinted with permissions from *John Wiley and Sons* for (A and B) Ref. [321], *American Chemical Society* for (C) Ref. [322], *Elsevier* for (D) Ref. [285].)

**Table 1.**

Antifouling ligands currently reported to protect UNMNPs *in vivo* from rapid MPS sequestration and enable efficient renal clearance

Surface ligand	Molecular structure	Hydrodynamic diameter	Liver accumulation	Renal clearance	Representative reference
Polyethylene glycol (PEG)-based		~5.5nm	~4% ID/g (24h p.i.)	>50% ID (24h p.i.)	Ref. [233]
Glutathione (GSH)		~3.3nm	~4% ID/g (24h p.i.)	>50% ID (24h p.i.)	Ref. [233]
Cysteinyglycine (Gly-Cys)		~3.1nm	~ 1.2 ID/g (24h p.i.)	~42% ID (24h p.i.)	Ref. [231]
Lipoic acid-based Sulfobetaine		~5nm	–	~70% ID (3hp.i.)	Ref. [231]
Dithiolated polyaminocarboxylate (DTDTPA)		~6.6nm	~6% ID/g (24h p.i.)	~60% ID (24h p.i.)	Ref. [257]